University of Zurich[UZH]

USZ Universitäts Spital Zürich

Master Thesis

Lars Widmer

MODELLING LYMPATHIC METASTATIC PROGRESSION IN ORAL CAVITY SQUAMOUS CELL CARCINOMA

---

supervised by

Dr. sc. nat. Roman Ludwig

Prof. Dr. rer. nat. Jan Unkelbach

at the

Department of Physics, UZH

Department of Radiation Oncology, University Hospital Zürich

28.09.2023, Zürich

Abstract

Radiotherapy plays a major role in the treatment of oral cavity squamous cell carcinoma (OCSCC). Because of the frequent spread to regional lymph nodes in the head and neck region, some parts of the neck are irradiated prophylactically in addition to the primary tumor and macroscopic lymph node levels. Current guidelines define this clinical target volume based on overall prevalences of lymph node metastases in the lymph node levels (LNL) and only partially consider the patient-specific clinical diagnosis. This work describes the observed lymph node involvement patterns and dependence on clinicopathological factors such as T-category and extension of the primary tumor over the mid-saggital plane, it further models the lymphatic metastatic progression in OCSCC patients with the help of a previously developed but further enhanced hidden Markov model that can estimate the risk of microscopic disease in the LNLs given a individual patient's clinical diagnosis. Based on the model's risk predictions a more personalized elective target volume definition is supported. Our analysis showed the possibility of sparing ipsilateral LNL III for a clinically classified N0 patient and contralateral LNLs in patients without a primary tumor extending over the mid-saggital plane. Additionally, LNL IV is rarely involved on the ipsilateral and contralateral side. Therefore, the model may support future clinical trials on volume de-escalation strategies in radiotherapy of OCSCC patients.

Contents

Chapter 1

Introduction

This thesis extens previous work on modelling lymphatic metastatic progression in head and neck squamous cell carcinomas (HNSCCs). The Hidden Markov Model (HMM) proposed by Ludwig et al., which previously was applied to oropharyngeal HNSCC and was shown to allow risk estimation of microscopic LNL involvement [1]. In this thesis we now applied it to oral cavity HNSCC for a first time.

Head and neck cancer (HNC) includes tumors arising from the mucosal surfaces of the nasal and oral cavity, oropharynx, larynx and hypopharynx [2]. HNSCCs account for up to 90% of these tumors [3], making it the sixth most prevalent cancer worldwide [4]. Treatment of patients with HNSCCs is complex and is often done by combined modality therapy, including surgery, radiotherapy and chemotherapy [5]. Despite this multidisciplinary approach, 25% of patients develop recurrent cancer within 5 years [6]. Additionally, the impact of treatment on the quality of life is of crucial importance in HNSCCs, as it can include functional disturbances such as speech, swallowing, hearing and breathing [7].

As mentioned, radiotherapy plays a major role in the treatment of HNSCCs. However, the definition of the clinical target volume in the lymph node levels (CTV-N) is often based on general guidelines, which are mainly obtained from overall prevalences of lymph node involvement in large cohorts of a given primary tumor location and stage. [8, 9, 10, 11]. The stage is determined by the tumor-node-metastasis system (TNM) that categorizes the patient based on the size of the primary tumor (T-category: T1-T4), the involvement of the regional lymph nodes (N-category: N1-N3) and the presence of distant metastases (M-category: M0/M1). However, no information about the location of lymph node metastases is available based on the TNM classification. Therefore, a personalized approach for irradiation of HNSCC patients is only partly present in current guidelines and correlations between the lymph node involvement of different levels is not included. For example, with a prevelance of 12% on the

ipsilateral side, level III is irradiated in most cases for OCSCC patients. However, for different clinical diagnoses, the risk of occult disease in level III can be expected to vary strongly. For a clinically diagnosed N0 neck and a primary tumor in the gums for example the risk is expected to be much lower compared to a patient with clinically diagnosed metastases in LNL II and a primary tumor on the tongue. Low risk scenarios for occult disease could be identified by incorporating the patient's detailed clinical diagnosis for lymph node involvement in addition to the TNM classification and the primary tumor location. In a further extension, other patient specific risk factors like the extension of the tumor over the mid-sagittal plane (midline extension) could be included.

To quantify the risk of occult disease given a specific clinical diagnosis and in the consequence better individualize the CTV-N definition, a probabilistic Bayesian network model was developed by Pouymayou et al. [12]. Ludwig et al. [1] extended and improved the model by Pouymayou et al. [12] by modelling the lymphatic metastatic progression using HMM and including more patient information and primary tumor characteristics [13]. The ultimate goal is an application of such a model in clinical practice by being an aid for clinicians in safely reducing the extent of elective nodal treatment [14]. This could lead to quality of life improvement for the patients by reducing the probability of side effects [14].

The goal of the following work is to analyze the lymph node involvement of OCSCC patients and definining the differences for the different locations of the primary tumor (tongue, gums and cheek and floor of mouth) and involvement patterns as this information is only available to this extent for oropharyngeal squamous cell carcinoma (OPSCC) [15]. By applying the hidden Markov model by Ludwig et al. [1] to the oral cavity primary tumor location, analogous guidelines as for OPSCC patients could be proposed [13]. Additionally, possible model extensions could be developed based on specific data characteristics and relevant findings in a cohort of OCSCC patients.

Chapter 2

Patterns of lymph node involvement

The basis of this thesis on a data level is formed by a multicentric dataset of 348 retrospectively analyzed patients with newly diagnosed oral cavity squamous cell carcinoma treated at two institutions. Both, the Inselspital Bern and the Centre Léon Bérard in Lyon provided us a dataset including various tumor subsites including oral cavity, oropharynx, hypopharynx and larynx. Since only the prevalence for the involvement of individual LNLs has been reported for OCSCC up until now, it is important to also quantify the details of lymphatic progression patterns depending on the involvement of upstream LNLs, T-category, midline extension and extracapsular extension (ECE). Due to the additional fact that the Hidden Markov Model by Ludwig et al. [1] was never applied to the data of oral cavity squamous cell carcinoma patients, I will focus on the included 348 patients with a diagnosed primary tumor located in the oral cavity.

Additonally, this overview of the available information makes limitations in the data more clearly visible and could help to develop possible model extension ideas.

2.1 Head and neck squamous cell carcinoma

Epithelium, a pervasive tissue found on body surfaces and in cavities, including the skin and lungs, comprises three fundamental cell types: squamous, cuboidal, and columnar epithelial cells. Squamous cells are flat and thin, cuboidal cells are roughly as thick as they are wide, and columnar epithelial cells are tall and often hexagonal when viewed from above, densely packed with minimal intercellular space. [16]

Squamous cell carcinomas (SCCs) are malignancies originating from squamous cells within the epithelium as a result of specific mutations in epithelial stem cells responsible

for generating functional squamous cells. These cancers typically initiate in the basal lamina, where epithelial stem cells attach, as shown in figure 2.1. [13]

Given the prevalence of epithelium throughout the human body, SCCs can develop in various locations, including the lungs, skin, or cervix. However, they can also manifest within the mucosa of the oral and upper respiratory tract, resulting in head and neck squamous cell carcinoma (HNSCC). [13]

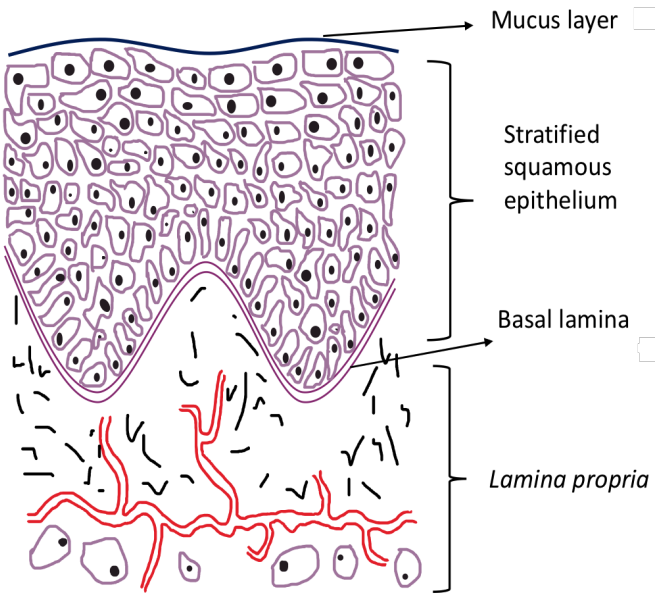

Figure 2.1: Schematic drawing ot the oral mucosa with its layers including the epithelium. [17]

2.2 Lymph system of the head and neck region

The lymphatic system is a vital component of the human body's circulatory system, running alongside the blood vessels in most tissues except for example the brain. It consists of a network of thin-walled capillaries that are highly permeable, allowing extracellular fluid, carrying waste products from cells, to drain into them. This fluid is transported back into the bloodstream through the thoracic duct. [18, 19, 20]

In addition to capillaries, the lymphatic system includes organs and structures crucial to the immune response. Lymph nodes, situated at junctions of afferent lymphatic vessels, play a central role. Incoming fluid passes through these nodes, where immune cells like

lymphocytes and macrophages come into contact with particles carried by the fluid. Ultimately, the fluid exits through efferent lymphatic vessels at the lymph node's hilus. [18, 21]

In the head and neck region, the lymphatic system consists of around 300 lymph nodes [22], categorized into lymph node levels (LNLs) for standardized reference. These boundaries, defined by identifiable anatomical landmarks such as bones, muscles, blood vessels, or nerves, serve as a reference for medical procedures, including neck dissections and radiotherapy [23, 24].

Head and neck squamous cell carcinoma (HNSCC) tumors have the potential to shed live cells into the lymphatic fluid. These cells can enter lymph nodes, where factors unique to SCCs allow them to evade programmed cell death processes [25]. Once inside a lymph node, these cells may proliferate, forming metastatic lesions. Subsequently, metastatic lesions can shed more tumor cells that can flow further downstream within the lymphatic system, leading to additional growth.

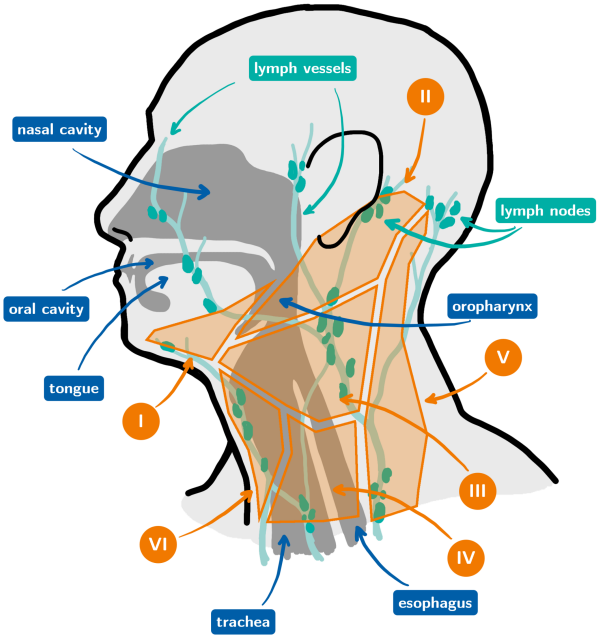

Figure 2.2: Schematic drawing of the head and neck region and its lymphatic network. The lymph nodes and vessels are shown in green, the primary tumor subsites (e.g oral cavity) in blue and the LNLs in orange. [13]

The presence of lymph node metastasis significantly impacts the prognosis of HNSCC

patients, with a notably lower survival rate. Therefore, it is considered one of the most critical prognostic factors for HNSCC. [26, 27, 28]

This comprehensive understanding of the lymphatic system's role in HNSCC progression and metastasis is invaluable in clinical diagnosis, staging, and the development of treatment strategies for this type of cancer.

2.3 Modalities

For all 348 patients, the lymph node involvement was recorded based on pathology following neck dissection. When possible, the involvement was specified for every individual level from I-V. However, the patient cohort from the Inselspital Bern contained 179 patients that had at least two levels dissected together while this was not the case for the cohort from Lyon. Additionally, the Inselspital Bern provided clinical diagnoses of lymph node metastases based on CT, MRI and PET scans for its 202 patients. In the table 2.1 an overview over the available data is given.

Table 2.1: Overview of the available modalities and the number of patients they are available for in the respective cohort.

Modality	Center	
	Bern	Lyon
CT	24 (12%)	0 (0%)
MRI	173 (86%)	0 (0%)
PET	112 (55%)	0 (0%)
Pathology	202 (100%)	146 (100%)
Total	202 (100%)	146 (100%)

One can see, that only pathology information is available for all patients in both datasets. Clinical diagnoses based on CT scans are only provided for 24 patients in the cohort from Bern, while involvement information based on MRI and PET scans includes the majority of 202 patients (86% and 55%). For the cohort from Lyon, only pathology information is recorded for all patients. Since both datasets include comprehensive information for lymph node level involvement based on pathology (after neck dissection), they are believed to be comparable and therefore are combined into a larger cohort for further analysis. This decision is also supported by section 2.4

2.4 Comparison of datasets

As shown in table 2.2, the CLB dataset has approximately the same number of early (T1/T2) and late (T3/T3) T-category tumors (early: 51%, late: 49%) while the ISB dataset has significantly more early T-category tumors with 74%. The largest difference can be observed for T1 which is observed way less in the CLB dataset (14% vs. 43%). The opposite case is then observed for T4 where there are fewer tumors in the ISB dataset. The differences may be explained by patient selection due to referral patterns. This possibly leads to the larger cohort of N+ patients in the CLB dataset (57%) compared to the ISB dataset (46%). Consistency over the two datasets can be observed for the involvement of the lymph node levels. The individual comparisons for the datasets regarding the involvement patterns can be looked at on LyProX [29]. The dataviewer with the selected patients can be seen in figure 2.3.

Table 2.2: Comparison of the dataset from the Inselspital Bern (ISB) and the Centre Léon Bérard (CLB)

	Dataset	
Staging	ISB	CLB
T1	86 (43%)	21 (14%)
T2	64 (32%)	54 (37%)
T3	17 (8%)	28 (19%)
T4	35 (17%)	43 (29%)
Early	150 (74%)	75 (51%)
Late	52 (26%)	71 (49%)
N+	87 (43%)	83 (57%)
Total	202	146

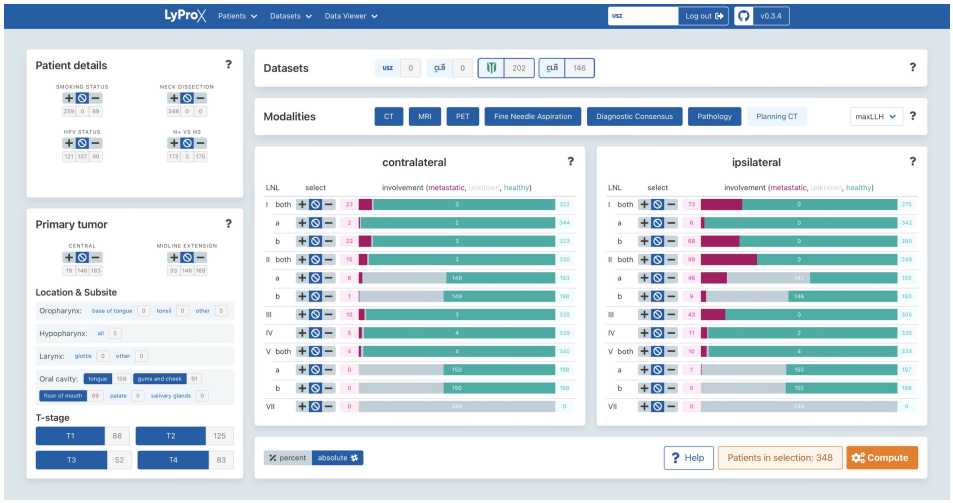

Figure 2.3: LyProX online interface to visualize the patterns of lymphatic progression in head and neck squamous cell carcinoma.

2.5 Subsites and T-stage

In addition the T-stage and the subsite in the oral cavity are available for all patients. In table 2.3, the T-stage distribution for every T-stage is shown.

Table 2.3: Patient cohort stratified for subsite and T-stage.

T-stage	Subsite			Total
	Tongue	Gums & Cheek	Floor of Mouth	
T1	55 (35%)	24 (26%)	28 (28%)	107 (31%)
T2	72 (46%)	15 (16%)	31 (31%)	118 (34%)
Early	127 (80%)	39 (43%)	59 (60%)	225 (65%)
T3	27 (17%)	6 (7%)	12 (12%)	45 (13%)
T4	4 (3%)	46 (51%)	28 (28%)	78 (22%)
Late	31 (20%)	52 (57%)	40 (40%)	123 (35%)
Total	158 (45%)	91 (26%)	99 (28%)	348 (100%)

The subsite with the most patients is tongue (C02[1]) with almost 50% of all patients, while gums and cheek (C03, C06[1]) and floor of mouth both include approximately 25%.

[1]Definition of the primary tumor location according to the international classification of diseases for oncology: ICD-O [30]

In total, there are more early than late T-stage tumors. However, when looking at the subsites, this is not the case for gums and cheek where the majority of the patients has a T4 tumor. While tumors in the tongue region almost never reach T4 before being diagnosed, T3 is rarely observed in the gums and cheek subsite. For floor of mouth (C04[1]), the distribution among the T-stages is more uniform.

2.6 Lymph node involvement

2.6.1 Involvement of individual LNLs

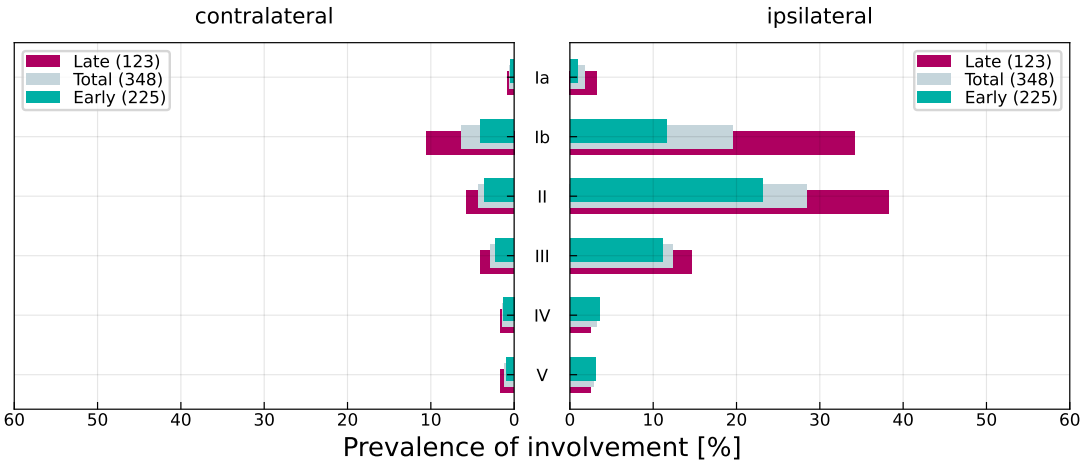

Figure 2.4: Contralateral and ipsilateral prevalence for the individual LNLs (I-V) stratified by T-category (early: T1/T2, late: T3/T4, total: T1-T4)

In figure 2.4 the prevalence of LNL involvement is compared for all oral cavity patients based on their T-category (early: T1/T2, late: T3/T4) for both the ipsilateral and contralateral side. Additionally, the overall prevalence, independent of the T-category, is included. As expected, the involvement on the contralateral side is in all LNLs significantly lower than on the ipsilateral side. For late T-category patients, the same is ovserved on both sides for levels with high involvement (Ib, II and III). The prevalences for level Ib, II and III increased from 12%, 23% and 11% to 34%, 38% and 15% on the ipsilateral side and from 4%, 4% and 2% to 11%, 6% and 4% on the contralateral side. Levels Ia, IV and V with overall lower prevalence showed smaller differences. The overall prevalence shows the weighted average of the prevalence for the early and late T-category.

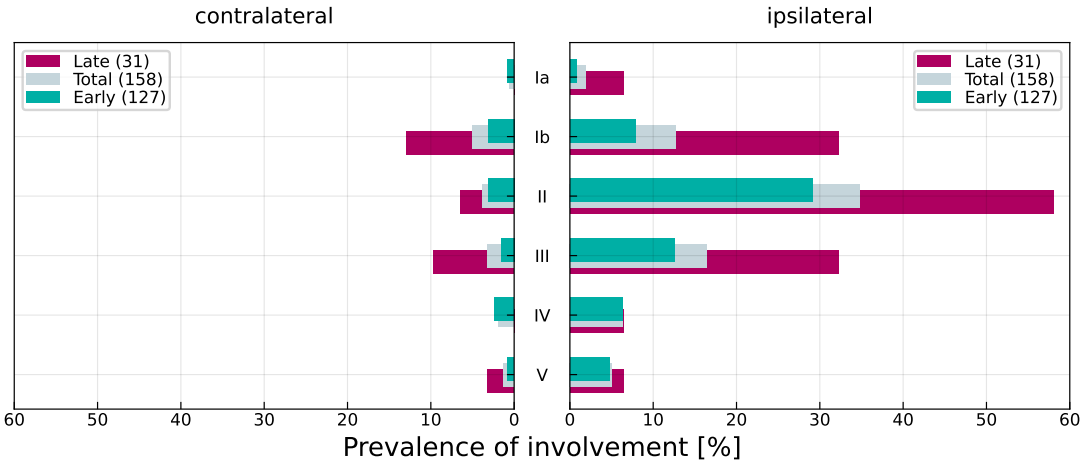

(a) Tongue

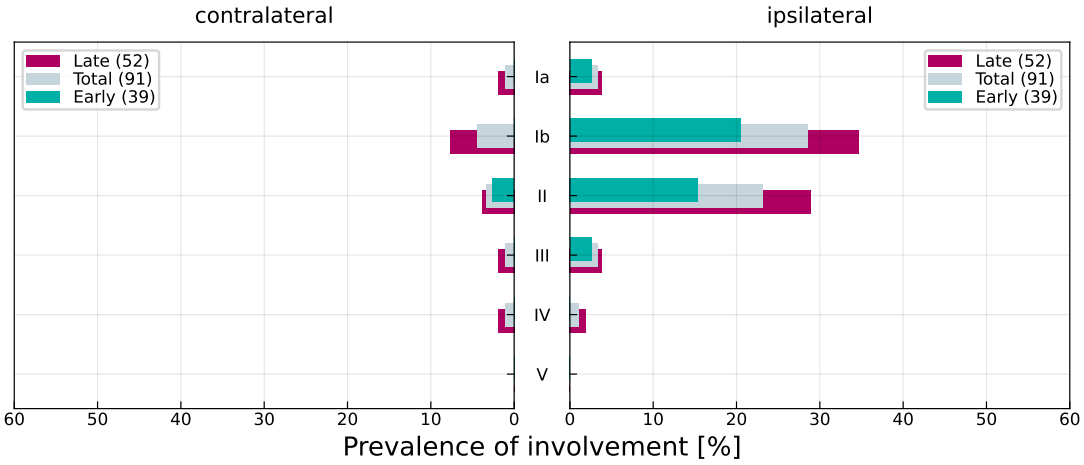

(b) Gums and cheek

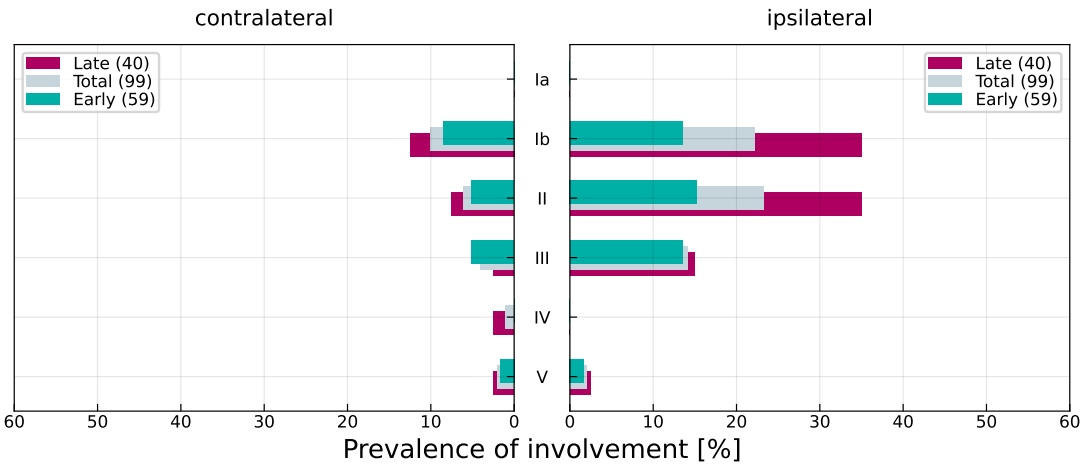

(c) Floor of mouth

Figure 2.5: Contralateral and ipsilateral prevalence for the individual LNLs (I-V) stratified by T-category (early: T1/T2, late: T3/T4, total: T1-T4) for the three subsites ((a): Tongue, (b): Gums and cheek, (c): Floor of mouth) of the oral cavity.

Table 2.4: Prevalence of the individual LNLs for all patients, stratified by T-category, tumor subsite, extracapsular extension and N+ staging.

		Total	I		II		III		IV		V	
		Value	Value	%	Value	%	Value	%	Value	%	Value	%
ipsi	all	348	73	21	99	28	43	12	11	3	10	3
	T1/T2	225	30	13	52	23	25	11	8	4	7	3
	T3/T4	123	43	35	47	38	18	15	3	2	3	2
	tongue	158	23	15	55	35	26	16	10	6	8	5
	gums & cheeks	91	28	31	21	23	3	3	1	1	0	0
	floor of mouth	99	22	22	23	23	14	14	0	0	2	2
	N+	172	73	42	99	58	43	25	11	6	10	6
	ECE+	81	38	47	52	64	27	33	8	10	7	9
	ECE-	91	35	38	47	52	16	18	3	3	3	3
contra	all	348	22	6	15	4	10	3	5	1	4	1
	T1/T2	225	9	4	8	4	5	2	3	1	2	1
	T3/T4	123	13	11	7	6	5	4	2	2	2	2
	tongue	158	8	5	6	4	5	3	3	2	2	1
	gums & cheeks	91	4	4	3	3	1	1	1	0	0	0
	floor of mouth	99	10	10	6	6	4	4	1	1	2	2
	N+	172	22	13	15	9	10	6	5	3	4	2
	ECE+	81	8	10	9	11	7	9	5	6	3	4
	ECE-	91	14	15	6	7	3	3	0	0	1	1

Based on the differences observed T-stage distributions for the different subsites, the involvement of the individual lymph node levels should additionally be looked at on a subsite level and not for the oral cavity in total. In figure 2.5 the same analysis can be seen for the subsites tongue, gums and cheek and floor of mouth. It can be seen that the involvement patterns show some differences. On the ipsilateral side, Level II is more often involved for the subsite tongue (early: 29%, late: 58%) than for gums and cheek (early: 15%, late: 29%) and floor of mouth (early: 15% , late: 35%). The differences are smaller on the contralateral side but it can be said that gums and cheek shows the lowest involvement and almost none for early T-category patients.
In the table 2.4 the exact values from figure 2.4 and 2.5 are shown. Additonally, the involvement for the N+ patients, so the one with lymph node metastasis, is shown. The number of patients with involvement in a level naturally corresponds to the one in the category with all patients but the prevalence is approximately twice as high due to the fact that only 49% of all patients have an N+ staging. The last two rows of the ipsilateral and contralateral table 2.4 show the prevalence stratified for extracapsular

extension (ECE) in any level. ECE refers to the growth of a nodal cancer metastasis beyond the confines of the capsule of a lymph node into adjacent tissues [31]. ECE was only looked at for N+ patients as the N0 stage by definition has no extracapsular extension. One patient had no ECE information and was counted as negative. One can see that patients with ECE have a higher involvement on the ipsilateral side for all levels and the relative difference increases for level III, IV and V. As expected, on the contralateral side the involvement is lower and similar for ECE+ and ECE- in levels I and II. Again, for level III, IV and V, the relative difference between the two subgroups increases.

2.6.2 Patterns of lymph node involvement

In the previous subsection 2.6.1, the focus was layed on the prevalence in the individual LNLs. However as previously mentioned, even more important are the patterns of lymph node involvement that will be analysed in this subsection. It will be looked at how the presence of lymph node metastases in one level is affected by healty or involved adjacent and upstream levels.

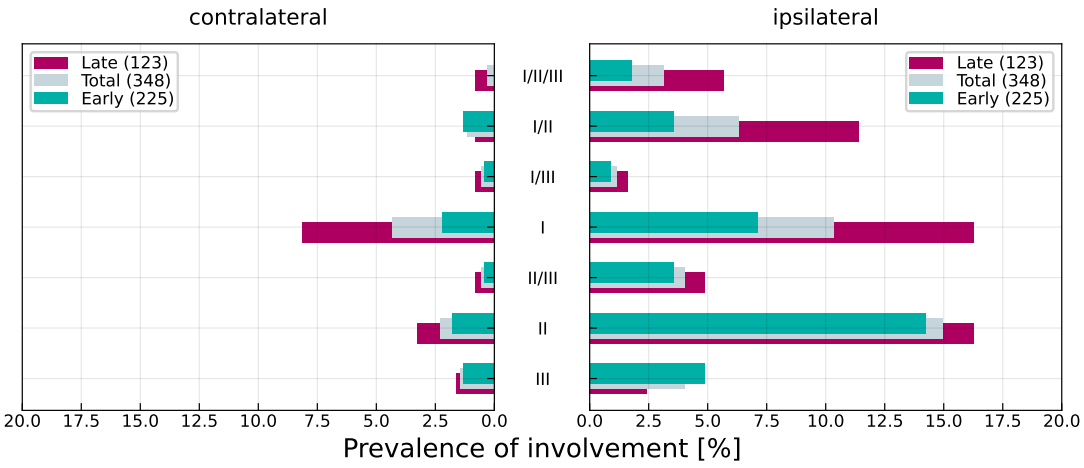

Figure 2.6: Contralateral and ipsilateral prevalence for the different involvement patterns of level I-III stratified by T-category (early: T1/T2, late: T3/T4, total: T1-T4). The labels show the involved levels (I-III). Level IV and V can be positive or negative.

In figure 2.6 the prevalence of the possible involvement patterns of levl I-III is shown for the ipsilateral and contralateral side stratified by T-category. The involvement of level IV and V is not considered since overall prevalence in these two levels is low as it has been shown in figure 2.4 and as downstream levels of level I-III their influence on the involvement on them is very limited.

It can be seen that the most common scenario for early T-category patients is to have involvement only in level II (14%) on the ipsilateral side and only in level I (2%) on the contralateral side. For late T-category patients, the cases where only level I or level II are equally prevalent (16%) on the ipsilateral side. On the contralateral side, only involvement of level I (8%) is the most frequent diagnosis. So there is substantial direct spread from the primary tumor to level I without level II or III being involved. However, there is still a substential co-involvement, especially with level II (I/II: 22 (30%)). The same applies to level II where overall on the ipsilateral side (early and late T-category) more than half (52 cases, 53%) of all patients with metastases in level II have no involvement of level I and III and 22% have co-involvement with level I (only I and II involved). For patients with metastases in level III co-involvement with level I and/or II is more often the case (29 cases, 67%). The full breakdown of co-involvement can be seen in table 2.5.

Additionally, the involvement of level I to III on the contralateral side is shown stratified for midline extension, as higher involvement is expected on the contralateral side when a tumor crosses the midline. This can be obsered when comparing the percentage of patients with no involvement in level I to III on the contralateral side for the two groups. 76% of all patients with midline extension hat no metastases in level I to III while for patients without midline extension it was 92%. As it shown in table 2.5, this difference is mainly because of higher involvement of level I individually when the tumor crosses the midline. So it can be said that midline extension is the most important risk factor for contralateral involvement.

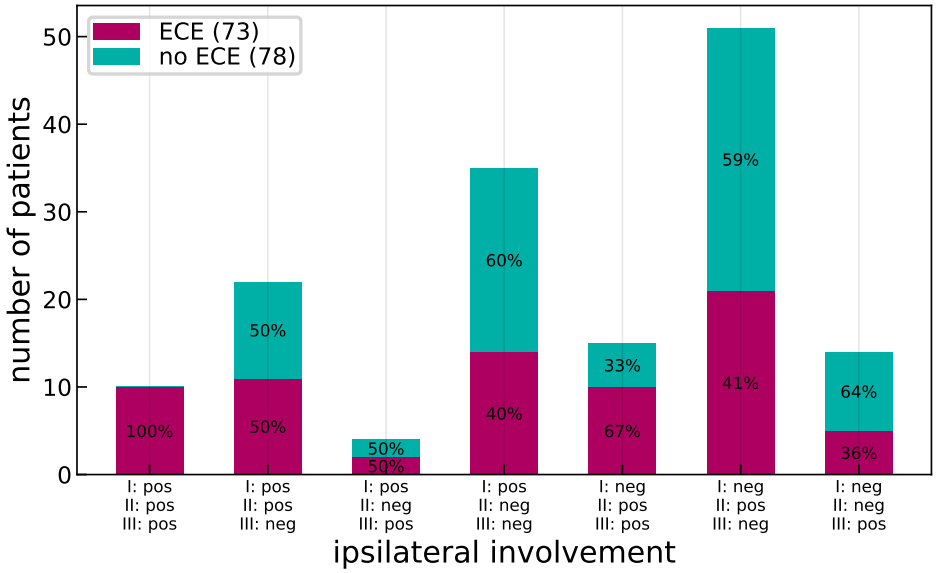

Figure 2.7: Simultaneous involvement of level I-III stratified by T-category (early: T1/T2, late: T3/T4, total: T1-T4). The labels show the involved levels (I-III). Level IV and V can be positive or negative.

The dependence of the ipsilateral involvement on the ECE can be seen in figure 2.7. ECE means that extracapsular extension was found in any level on the ipsilateral or contralateral side. Only N+ patients are included as per definition only these can have ECE. It can be seen that for patients with ECE states with more advanced lymph node involvement (more than one level involved) are more often observed while for patients without ECE, the states with only one lymph node level involved are more frequent (e.g I: pos, II/III: neg). The state with all three lymph node levels involved (I-III) is only observed for patients with ECE.

Table 2.5: Prevalence of the lymph node patterns of level I to III for all patients, stratified by T-category and ECE for both the ipsilateral and contralateral side. For the contralateral side, additionally the stratification for midline extension is shown.

		I/II/III		I/II		I/III		I		II/III		II		III		no I/II/III	
		Value	%	Value	%	Value	%	Value	%	Value	%	Value	%	Value	%	Value	%
ipsi	all	11	3	22	6	4	1	36	10	14	4	52	15	14	4	195	56
	T1/T2	4	2	8	4	2	1	16	7	8	4	32	14	11	5	144	64
	T3/T4	7	6	14	11	2	2	20	16	6	5	20	16	3	2	51	41
	ECE+	11	14	11	14	2	2	14	17	9	11	21	26	5	6	8	10
	ECE-	0	0	11	12	2	2	22	24	5	5	31	34	9	10	11	12
contra	all	1	0	4	1	2	1	15	4	2	1	8	2	5	1	311	89
	T1/T2	0	0	3	1	1	0	5	2	1	0	4	1	3	1	208	92
	T3/T4	1	1	1	1	1	1	10	8	1	1	4	3	2	2	103	84
	ECE+	1	1	2	2	0	0	5	6	2	2	3	4	4	5	64	79
	ECE-	0	0	2	2	2	2	10	11	0	0	4	4	1	1	72	79
	Mid+	0	0	0	0	0	0	6	18	1	3	1	3	0	0	25	76
	Mid-	0	0	2	1	0	0	6	4	0	0	3	2	3	2	152	92
	Mid?	1	1	2	1	2	1	4	3	1	2	4	3	2	1	130	89

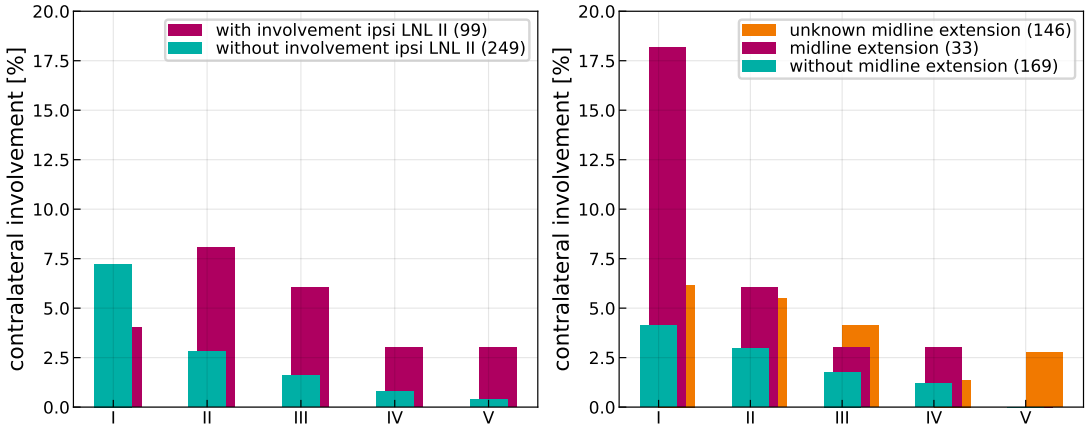

Figure 2.8: Involvement in the contralateral level I-V stratified for involvement of ipsilateral level II (left) and midline extension (right).

In figure 2.8 the involvement in the contralateral levels can be seen given involvement or no involvement of ipsilateral level II (left) and given midline extension or no midline extension (right). One can see that given involvement of ipsilateral level II, the contralateral involvement is higher in every level except level I compared to the case where ipsilateral level II is not involved. So contralateral involvement for levels II to V is reare when ipsilateral level II is not involved. The same applies even for midline extension. For the involvement of contralateral level I, midline extension even increases the prevalence of metastases by over 10%. In the levels II to IV the difference is smaller but still present. In total 33 (17%) out of 202 patients had a tumor extending over the midline. For 146 patients, namely the patients in the CLB dataset, the midline extension was unknown. The prevalence in the contralateral levels I, II and IV for patients with unknown midline extension is in between the prevalence of midline extension and no midline extension. This is expected as the CLB dataset that has no midline extension information assumingly contains approximately a similar percentage of patients with tumors extending the midline. Higher involvement in contralateral level III and especially V could be explained by the more late T-category patients in the CLB dataset.

2.6.3 Positive versus investigated lymph nodes

In figure 2.9 the number of pathologically positive lymph nodes can be seen in dependence of the number of dissected lymph nodes. It is shown for the levels Ib, II and III. Ia and Ib are separated since they show different involvement as already mentioned (2.4). For level Ia there is not enough pathological data available for a sophisticated analysis. This is due to the fact that in many patients several lymph node levels are dissected

together, making it impossible to assign the lymph nodes to the correct level. Therefore, also in the level II and III the respective patients are excluded, leading to different number of included patients for every level. The analysis for the contralateral side is not separately shown but has similar characteristics as the here described ipsilateral side.

The most apparent characteristic is the large variability in the number of lymph nodes observed between patients. The largest span is observed in level II with 0 to 42 lymph nodes. For level III the span is smaller with 0 to 30, while level Ib shows the smallest range including 0 to 16. This leads to a difference in the mean number of investigated lymph nodes between the levels (Ib: 4, II: 13, III: 8). Looking at the histograms next to the y-axis in figure 2.9, one can see that in most cases a patient has only 1 positive lymph node in the involved level. No more than 6 positive lymph nodes are observed in any patient in level Ib and II, while for level III the maximum was 4. More than 1 positive lymph node was observed for 22 patients (7%) in level Ib, 35 patients in level II (11%) and only 11 patients in level III (3%).

The analysis on wheter the probability of having at least one positive lymph node increases with the number of lymph nodes present in a patient, can be seen in figure 2.10. Patients with zero lymph nodes are excluded and the analysis is based on a linear regression with the binary predicted variable (y) being involvement/no involvement. The explanatory variable is the number of lymph nodes investigated. One can see that an increase in lymph nodes is associated with a slightly higher probability of involvement in level Ib, II and III on the ipsilateral side. However, when looking at the 95% confidence interval of the slope parameter that represents the increase of the probability of involvement per additional lymph node, one can see that also negative slopes are included for level II and III. Only for level Ib there is a possibility of a slight positive correlation between the probability of involvement and the number of lymph nodes. However, overall there is no significant evidence present that the probability of involvement increases with the number of lymph nodes a patient has and the 95% confidence intervals include the average involvement for every number of dissected lymph nodes.

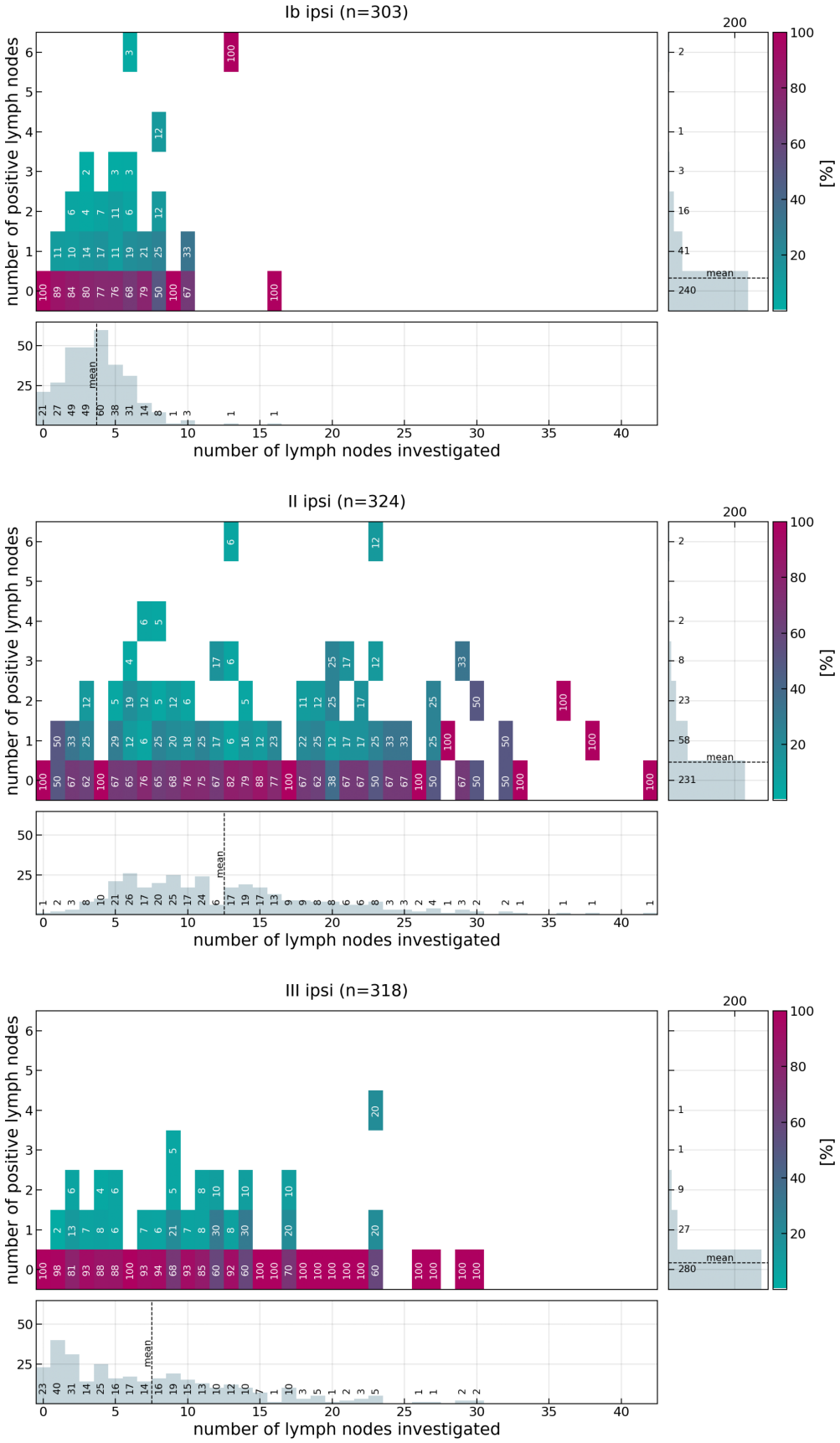

Figure 2.9: Histogram of the number of pathologically investigated and positive lymph nodes in the levels Ib, II and III on the ipsilateral side. Patients were excluded level-wise if there was no pathological information.

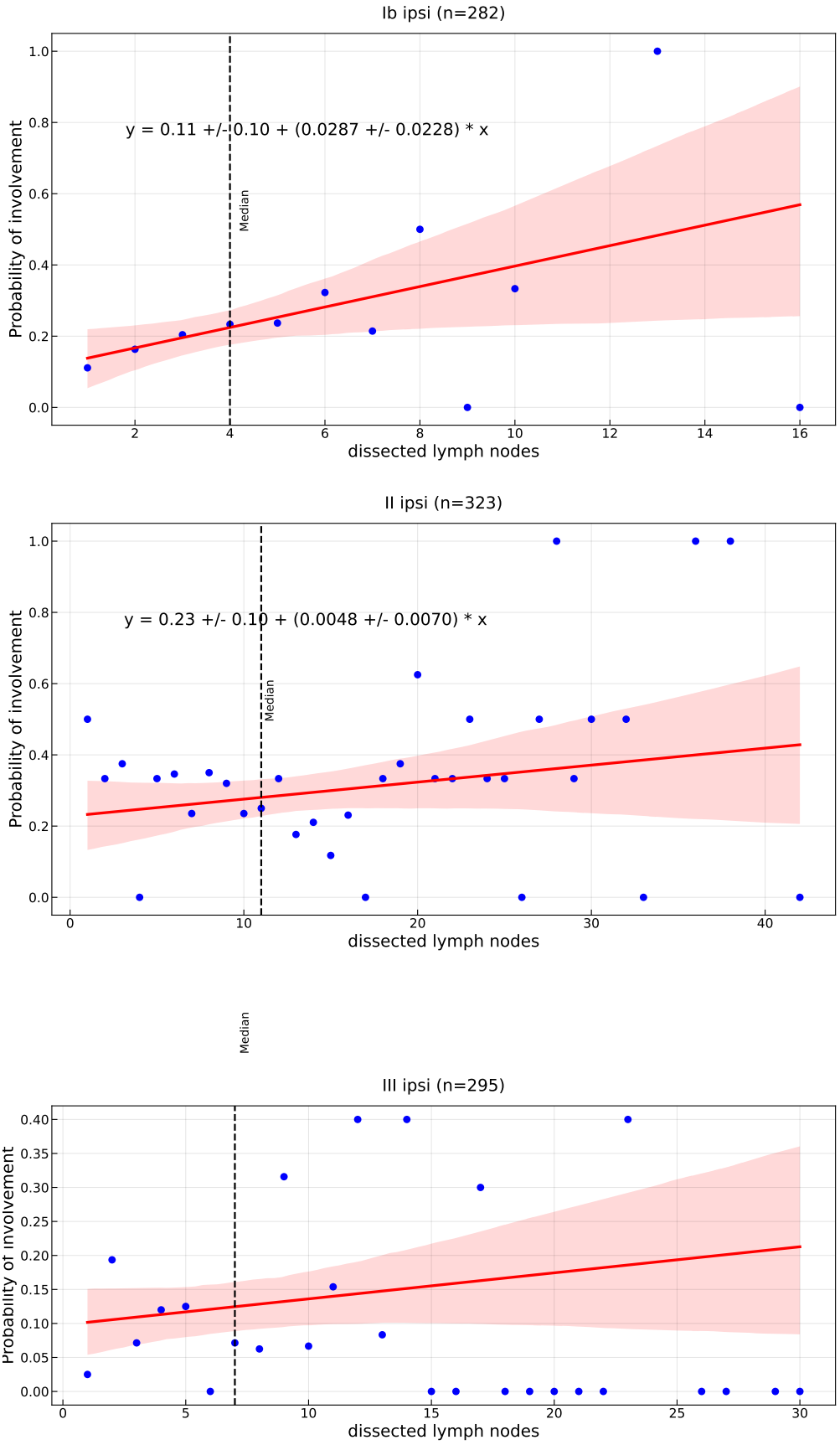

Figure 2.10: Linear regression with 95% confidence interval for the prediction of the probability of involvement in dependence of the number of lymph nodes in a level and patient. The blue dots represent the observed involvement. The median line shows the median number of lymph nodes found in a patient and LNL.

2.7 Conclusion

The goal of this chapter was to analyze the level wise lymph node involvement for OC-SCC patients. The dependence on the primary tumor subsite, T-category, involvement of adjacent and nearby lymph node levels, ECE and extension of the primary tumor over the midline has been shown. Additionally, the available raw pathology data was presented in figure 2.9.

The most important findings include:

- **Differences in the T-catergory distributions** for the different oral cavity subsites. Especially gums and cheek has a majority of patients with a T4 tumor. This indicates a longer time span of tumor growth until the time of diagnosis.
- **Involvement on the contralateral side is much lower** than on the ipsilateral side and increases with higher ipsilateral involvement and midline extension. This can be explained by the increase in possible spread from the primary tumor.
- **Late T-category** patients tend to show **higher involvement** on the ipsilateral and contralateral side. Involvement in lymph node level Ib and II shows the highest prevalence for involvement. Level Ia, IV and V show very low involvement.
- **ECE** shows no significant difference in level I and II. For level III, IV and V the relative differences of involvement increase. However, states with more advanced lymph node involvement are more frequent in patients with ECE.
- There is substantial **co-involvement** in between levels I, II and III, as level I is frequently involved in combination with level II (22%) and level III is co-involved with level I and/or II in 67% of the cases.
- There is a **large variability** in the **number of lymph nodes** between patients. However, there is **no significant evidence** for an **increased risk** of involvement when a patient has more lymph nodes. Additionally, the mean number of investigated lymph nodes varies between the levels.

In comparison with previous studies, the reported prevalences in the individual lymph node levels (2.4) are similar to the ones reported in the study by Grégoire et al. [32] that reported 15%, 28%, 6%, 2% and <1% for level Ib, II, III, IV and V on the ipsilateral side in 787 OCSCC patients. The differences, for example in level III, could arise due to variations in the patient selection such as different subsite compositions and T-stage distribution. This is supported by similar patterns observed for the lymph node involvement in the different subsites (tongue, gums and cheek and floor of mouth) (figure 2.5, [32]).

2.7.1 Limitations and bias

Limitations in the datasets include possible difference in the surgical differentiation of the lymph node levels at the two institutions. Especially in level II and III the mean number of lymph nodes varies between the datasets (CLB: 4, 11 ISB: 9, 17). This could lead to differences in the allocation of metastases to the lymph node levels, resulting in different involvement patterns.

A potential bias in both datasets is that contralateral neck dissection is not performed for all patients. This could induce an underestimation of microscopic metastasis on the contralateral side resulting in too low prevalences for the lymph node involvement.

2.7.2 Potential impact on elective nodal irradiation and neck dissection

The data presented in the previous chapter shows a low occurrence of lymph node metastases in levels IV and V, thereby advocating for the consideration of excluding these levels in neck dissection and elective nodal irradiation. Specifically, in cases where level III is not involved, the likelihood of level IV involvement is considerably low. The described low contralateral involvement could support the unilateral treatment of the neck in patients with tumors not crossing the midline (Mid-) and low ipsilateral involvement.

The analyzed dependencies of the involvement of level I-III on T-category, metastases in adjacent lymph node levels and tumor subsite could also have an influence on the elective treatment. However, to give statistically significant treatment recommendations, probabilistic models are needed to quantify the conditional risk of occult disease in a level for specific clinical diagnoses of lymph node involvement and other clinicopathological factors. To obtain these results, the hidden Markov model proposed by Ludwig et al. [1], that also implements specificity and sensitivity for the clinical diagnoses, will be applied to the described multicentric dataset.

Chapter 3

Unilateral hidden Markov model

Following chapter 2 and the conclusions that the involvement and elective treatment decision of lymph node level I-III could be dependent on the T-category and metastases in adjacent lymph node levels, the mentioned hidden Markov model [1] will now be applied to the OCSCC dataset. In a first step a unilateral model that only considers and predicts ipsilateral involvement will be trained and analyzed. In the following sections, this base model will be introduced and optimized.

3.1 Mathematical description

Before treatment, a patient is always clinically diagnosed. Based on imaging modalities, such as MRI, CT and PET, the primary tumor and possible lymph node metastases are located. However, the clinical diagnosis can include false positive and false negative cases. This means that for example a metastasis can be clinically diagnosed even though in reality there is no involvement present in this lymph node level. Therefore the true state is not observable and hence hidden. An advantage of the hidden Markov model is, that it can model these observed and hidden states of the LNLs with binary random variables.

For the hidden (true) state we have:

$$X_v \in \{0, 1\} \quad \text{for} \quad v \in \{1, 2, \dots, V\} \tag{3.1}$$

Where v indexes the V included LNLs. $X_v = 0$ corresponds to a healthy LNL, while $X_v = 1$ represents involvement in LNL v.

For the observed states the representation follows the same principle but now we have an observed random variable $Z_v^{\mathcal{O}}$ for every available modality $\mathcal{O} \in \{MRI, CT, \dots\}$.

$$Z_v^{\mathcal{O}} \in \{0, 1\} \quad \text{for} \quad v \in \{1, 2, \dots, V\}, \quad \mathcal{O} \in \{MRI, CT, \dots\} \tag{3.2}$$

The observed random variable states if given X_v the used modality $\mathcal{O}$ with specificity $s_P^{\mathcal{O}}$ and sensitivity $s_N^{\mathcal{O}}$ results in observing metastases ($Z_v^{\mathcal{O}} = 1$) or not ($Z_v^{\mathcal{O}} = 0$).

For convenience, we write the random variables in a vector:

$$\begin{aligned} \text{observed vector} \quad & \boldsymbol{Z} = (Z_v) \to \{0,1\}^V \\ \text{hidden vector} \quad & \boldsymbol{X} = (X_v) \to \{0,1\}^V \end{aligned} \tag{3.3}$$

The conditional probabilities of observing a diagnosis $Z = z$ for a given state $X = x$ of a lymph node level are then:

$$\begin{aligned} P(Z = 0 \mid X = 0) &= s_P \\ P(Z = 1 \mid X = 0) &= 1 - s_P \\ P(Z = 1 \mid X = 1) &= s_N \\ P(Z = 0 \mid X = 1) &= 1 - s_N \end{aligned} \tag{3.4}$$

A second advantage, compared for example to a Bayesian Network model, is that the lymphatic progression over time can be defined by a hidden Markov model. The previously defined hidden random vector (eq. 3.3) is therefore time dependent:

$$\boldsymbol{X}[t] = (X_v[t]) \quad \text{for} \quad t \in \{0, 1, 2, \ldots, t_{max}\} \tag{3.5}$$

The time-steps are discrete and reach t_{max}. For the diagnosis $\boldsymbol{Z}$ on the other hand, there is just an observation at the point of the cancer diagnosis, hence making a time differentiation unnecessary.

With the time dependence of the hidden state and the conditional probabilities of observing a diagnosis given the true state of the lymph node level, we can fully describe the hidden Markov model starting in a state $\boldsymbol{X}[t = 0] := \boldsymbol{\pi}$. The starting state $\boldsymbol{\pi}$ is the point where the patient is still healthy. Therefore we have:

$$\boldsymbol{\pi} = \begin{bmatrix} 0 \\ 0 \\ \vdots \\ 0 \end{bmatrix} \tag{3.6}$$

The conditional probability of the progression from state $\boldsymbol{X}[t]$ to a state $\boldsymbol{X}[t+1]$:

$$P(\boldsymbol{X}[t+1] \mid \boldsymbol{X}[t]) \tag{3.7}$$

and the probability of an observation given the true hidden state of the LNL:

$$P(\boldsymbol{Z} \mid \boldsymbol{X}[t]) \tag{3.8}$$

To model the transition probabilities from one state to another, we have to introduce a graph that defines our hidden Markov model. It reflects the lymphatic system with its defined LNLs and the resulting tumor spread patterns. An example of such a graph can be seen in figure 3.1

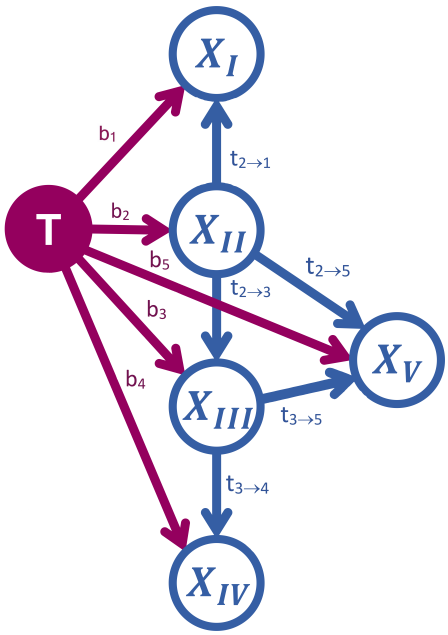

Figure 3.1: Hidden Markov model represented as a graph to show lymphatic spread in the LNLs.

The graph is represented by edges and directed arcs. The edges represent the primary tumor **T** and the hidden binary variables X_v specifying the involvement of LNL v. The directed arcs are a surrogate of the lymphatic flow and the parameter next to each arc represents the probability rate for lymphathic spread in this direction. These parameters can be used to explicitly write down the conditional probabilities introduced in eq. 3.7:

$$
\begin{aligned}
P(X_v[t+1]=0 \mid X_{pa(v)}[t]=0) &= Q(X_v[t+1]=0; X_v[t]) \times (1-b_v)^{1-X_v[t]} \\
P(X_v[t+1]=1 \mid X_{pa(v)}[t]=0) &= Q(X_v[t+1]=1; X_v[t]) \times (b_v)^{1-X_v[t]} \\
P(X_v[t+1]=0 \mid X_{pa(v)}[t]=1) &= Q(X_v[t+1]=0; X_v[t]) \\
&\quad \times ((1-b_v)(1-t_{pa(v)\to v}))^{1-X_v[t]} \\
P(X_v[t+1]=1 \mid X_{pa(v)}[t]=1) &= Q(X_v[t+1]=1; X_v[t]) \\
&\quad \times (1-(1-b_v)(1-t_{pa(v)\to v}))^{1-X_v[t]}
\end{aligned}
\tag{3.9}
$$

Where $pa(v)$ is the parent node of v and Q is a term formalizing the fact that a metatastatic LNL cannot become healthy again as time progresses. Therefore, Q is always 1, except for the case where $X_v[t+1]=0$ and $X_v[t]=1$, where it is 0. Using one minus the node's previous value ensures thath the probability of the node to stay involved is 1.

Following the same principle, the probabilities in eq. 3.9 can be extended for the more general case where a LNL has multiple parent nodes:

$$
\begin{aligned}
P(X_v[t+1]=x_v \mid &\{X_r[t]=x_r, t_{rv}\}_{r\in pa(v)}, b_v) \\
&= Q(X_v[t+1]=x_v; X_v[t]) \times (x_v + (-1)^{x_v} \\
&\quad (1-b_v) \prod_{r\in pa(v)} (1-t_{rv})^{x_r})^{1-X_v[t]}
\end{aligned}
\tag{3.10}
$$

In order to receive the probability of the whole patient state $\boldsymbol{X}[t+1]$, we can simply take the product over all individual LNLs that are each described by eq. 3.10. For simplicity, from now on we will mostly write $P(X=x)$ as just $P(x)$.

$$
P(\boldsymbol{x}[t+1] \mid \boldsymbol{x}[t]) = \prod_{v\le V} P(X_v[t+1]=x_v \mid \{X_r[t]=x_r, t_{rv}\}_{r\in pa(v)}, b_v) \tag{3.11}
$$

Evaluating eq. 3.11 for all possible combinations of the states ($\boldsymbol{x}$) creates a square matrix $\boldsymbol{A}$, called the transition matrix. It contains the probability of all individual state transitions during a timestep. Because of the forbidden self-healing, many entries of the transition matrix are 0.

As our main goal is to learn the probability rates assigned to the arcs in figure 3.1, we need to calculate the likelihood function. The likelihood tells us how likely it is to observe the given data based on the assigned probability rates. Therefore, we have to

define an observation matrix $\boldsymbol{B}$ that can include the patients clinical diagnosis. The calculation of this observation follows the same principle as the transition matrix and is specified via sensitivity and specificity as shown in eq. 3.4.

$$\boldsymbol{B} = P(\boldsymbol{Z} = \boldsymbol{\zeta_i} \mid \boldsymbol{X}[t] = \boldsymbol{\xi_i}) \tag{3.12}$$

Since we only have an observation of the patient state at the point of diagnosis, we don't know the evolution of the patient's disease. So we have to marginalize over all possible paths that could lead to the observed diagnosis. In the hidden Markov formalism this is automatically obtained when multiplying the transition matrix with itself, followed by a multiplication with the observation matrix. The probability of observing a given diagnosis $\boldsymbol{z} = \boldsymbol{\zeta_j}$ at a fixed time-step can be therefore calculated as followed:

$$P(\boldsymbol{Z} = \boldsymbol{\zeta_j} \mid t) = [\boldsymbol{\pi}^T \cdot (\boldsymbol{A})^t \cdot \boldsymbol{B}]_j \tag{3.13}$$

Where $\boldsymbol{\pi}$ is the vector for the healthy starting state. The index j ensures that the component corresponding to the diagnosis $\boldsymbol{Z} = \boldsymbol{\zeta_j}$ is taken from the resulting row-vector. This means that in this vector calculated with eq. 3.13 includes the probabilities for all possible diagnoses.

The next problem is, that the number of time-steps until the diagnosis is not known. So we have to marginalize over the discrete number of time-steps at which the cancer could be diagnosed. In order to do this. a time-prior $p(t)$ has to be introduced, that describes the prior probability that the diagnosis happens at a specific time-step t. In our case this discrete distribution over the finite number of time-steps is a binomial distribution.

Implementing this time-prior also directly allows us to incorporate the T-category of the patients into the likelihood function. The importance of this has been shown in the previous chapter where a difference in involvement between early and late T-category patients was observed. By taking the sum over the defined number of time-steps and the product over all T-categories, we can eventually write down the **likelihood function**:

$$P(\boldsymbol{\mathcal{Z}} \mid \theta) = \prod_{T=1}^{T_{max}} \left[\sum_{t=0}^{t_{\max}} p_T(t) \cdot \boldsymbol{\pi}^\top \cdot (\boldsymbol{A})^t \cdot \boldsymbol{B} \right] \cdot \boldsymbol{f}_T \tag{3.14}$$

We no longer have a single diagnosis $\boldsymbol{Z} = \boldsymbol{\zeta_j}$ but the dataset $\boldsymbol{\mathcal{Z}}$ including all patients diagnosis. These diagnoses correspond to the observational state $\boldsymbol{\zeta}_j$ in eq. 3.13. That is also the reason why the index j is omitted to read out the probability for a specific state

and the column-vector $\boldsymbol{f}_T$ is added. $\boldsymbol{f}_T$ is defined separately for each T-category and specifies the number of patients that were diagnosed with the respective observational state and the given T-category. θ simply represents the model parameters, which are the probability rates shown in figure 3.1.

For computational reasons, mostly the log-likelihood is calculated instead of the likelihood. It can easily be obtained by taking the elementwise log of the sum-elements of the marginalization over the time-steps and summing over the T-categories:

$$\log P(\boldsymbol{\mathcal{Z}} \mid \theta) = \sum_{T=1}^{T_{max}} \log \left[\sum_{t=0}^{t_{\max}} p_T(t) \cdot \boldsymbol{\pi}^\top \cdot (\boldsymbol{A})^t \cdot \boldsymbol{B} \right] \cdot \boldsymbol{f}_T \tag{3.15}$$

A more sophisticated mathematical description, also including handling of incomplete diagnoses and multiple diagnostic modalities can be found in [13].

3.1.1 Sampling process

This subsection will shortly describe Markov-Chain Monte Carlo (MCMC) sampling that was also used in the sampling process of the model. A more sophisticated introduction into the topic can be found in Bishop [33], MacKay [34] or Gelman et al. [35].

We already derived the likelihood function $P(\boldsymbol{\mathcal{Z}} \mid \theta)$ shown in eq. 3.14 but given the dataset with its diagnoses, we want to know how th probability distribution $P(\theta \mid \boldsymbol{\mathcal{Z}})$ looks like. We can write this posterior distribution of the parameters using Bayes' rule:

$$P(\theta \mid \boldsymbol{\mathcal{Z}}) = \frac{P(\boldsymbol{\mathcal{Z}} \mid \theta) P(\theta)}{\int P(\boldsymbol{\mathcal{Z}} \mid \theta') P(\theta') \, d\theta'} \tag{3.16}$$

where $P(\theta)$ is the prior over these parameters. Since we have no information about the distribution of these parameters and are all probability rates, we choose a uniform prior that is defined on the inverval $[0, 1] \in \mathbb{R}$:

$$P(\theta) = \begin{cases} 1 & \text{if } \theta_a \in [0,1]; \forall a \leq E \\ 0 & \text{otherwise} \end{cases} \tag{3.17}$$

E is the number of edges in the graph shown in figure 3.1. The problem is that the normalization constant in the denominator can not be calculated analytically. MCMC sampling methods are an alternative to sample from the posterior $P(\theta \mid \boldsymbol{\mathcal{Z}})$ without calculating this normalization constant explicitly. We start constructing a Markov chain of samples $\theta_1, \theta_2, \ldots, \theta_\tau$ by drawing a new proposal $\theta^\star$ to add to the Markov chain. The proposal is drawn from the proposal distribution $q(\theta^\star \mid \theta_\tau)$ that depends on the

previous sample. The Metropolis algorithm is the easiest way to do this since the proposal distribution is symmetric ($q(\theta^\star \mid \theta_\tau) = q(\theta_\tau \mid \theta^\star)$) in this case. This new proposal is then accepted with a probability given by:

$$A\left(\theta^\star, \theta_\tau\right) = \min\left(1, \frac{P(\boldsymbol{\mathcal{Z}} \mid \theta^\star)P(\theta^\star)}{P(\boldsymbol{\mathcal{Z}} \mid \theta_\tau)P(\theta_\tau)}\right) \tag{3.18}$$

In this case we have the unnormalized posterior and do not need to calculate the normalization constant. If the proposal is accepted, $\theta_{\tau+1} = \theta^\star$ and otherwise the last sample is re-added to the chain $\theta_{\tau+1} = \theta_\tau$. By letting τ approach infinity and therefore repeating the described steps, the produced samples are distributed like the posterior $P(\theta)$.

The sampling implemented for the described model uses the *emcee* package [36] that uses a combination of two differential evolution algorithms [37] [38]. These refined methods, which determine the selection of the subsequent sample during the process, are primarily aimed at improving overall performance. The result of this process yields a collection of parameter samples $\tilde{\theta}$, whose density within the parameter space accurately represents the posterior distribution.

3.2 Application to OCSCC

In this section we apply the introduced model based on the graph in figure 3.1.

3.2.1 Data and model assumptions

As of now, we have a unilateral model that only considers the ipsilateral side of the patient where the primary tumor is located. Therefore, we include all 348 OCSCC patients, using the maximum likelihood consensus for their ipsilateral nodal involvement of the LNLs I to V. The maximum likelihood consensus considers the most likely state for a lymph node level based on all available diagnostic modalities and their respective sensitivity and specificity. A mathematical description for this consensus can be found in [13]. For this consensus the specificity (s_P) and sensitivity then (s_N) are fixed to 1, since pathological data is assumed to be the ground truth. For the risk predictions in section 3.2.3, the sensitivity was set to (s_N=81%) and the specificity to (s_P=76%), which represent the values for CT imaging according to Pouymayou et al. [12]. In order to give the model a sufficient number of time-steps to evolve and not let the probability rates be too small, t_{max} was set to 10. Regarding the T-category, we only distinguish between early (T1/T2) and late T-category (T3/T4) patients. The time prior $p(t)$ is a binomial distribution. In order to model the difference in involvement between early and late T-category patients, we have two binomial distributions each described by the

number of time-steps and the probability p_{late} and p_{early}. $p_{late} > p_{early}$ as we expect a late T-category patient to be diagnosed at a later time-step on average. Sampling of both parameters (p_{late}, p_{early}) is not possible because there would be no unique optimal choice. Therefore, $p_{early} = 0.3$ is fixed and only p_{late} is learned. The choice of this fixed value is somewhat arbitrary as mainly the relation of the two parameters is important. A visualization of the priors for the fixed p_{early} and an example for a sampled p_{late} can be seen in figure 3.2

The chosen graph described in figure 3.1 was shown to be the winning graph that can describe SCC patients the best by [13]. For the simple reason that there is no data available for LNL VII in the OCSCC dataset, connections to level VII are omitted.

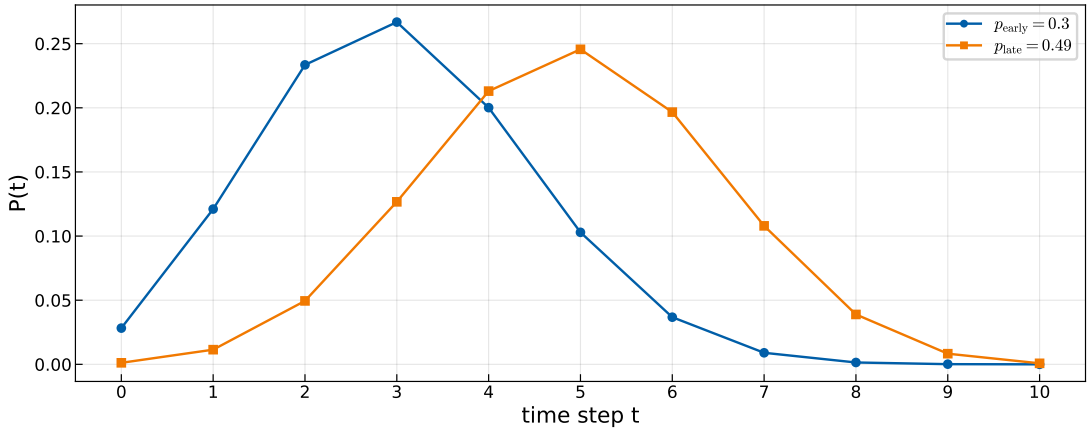

Figure 3.2: Visualization of the binomial time-priors for early and late T-category, showing the probability of a diagnosis at the specific time-steps.

3.2.2 Sampled parameters and predicted prevalences

In figure 3.3 you can see a corner plot of the sampled hidden Markov model parameters. On the diagonal, the histograms show the 1D marginals and on the lower triangle all possible combinations of 2D marginals for the model parameters are shown. The isolines enclose 20%, 50% and 80% of the sampled points respectively. Correlations between the parameters are low overall but can be seen for p_{late} with the spread from the primary tumor to the levels I, II and III. Additionally, there is a weak correlation between the parameter for the spread from level II to level I and the parameter for the spread from the primary tumor to level I. The exact absolute values of the parameters are not that important as they are dependent on the number of chosen time-steps and therefore also the fixed time prior for early T-category patients. However, we can now

model the evolution of the state of lymph node involvement over the time-steps. This allows us to calculate the probability of every possible state at every time-step. By marginalizing over the time-steps via the time-priors and summing over the relevant set of states, we can predict the prevalence for every possible involvement pattern or also involvement in an individual level.

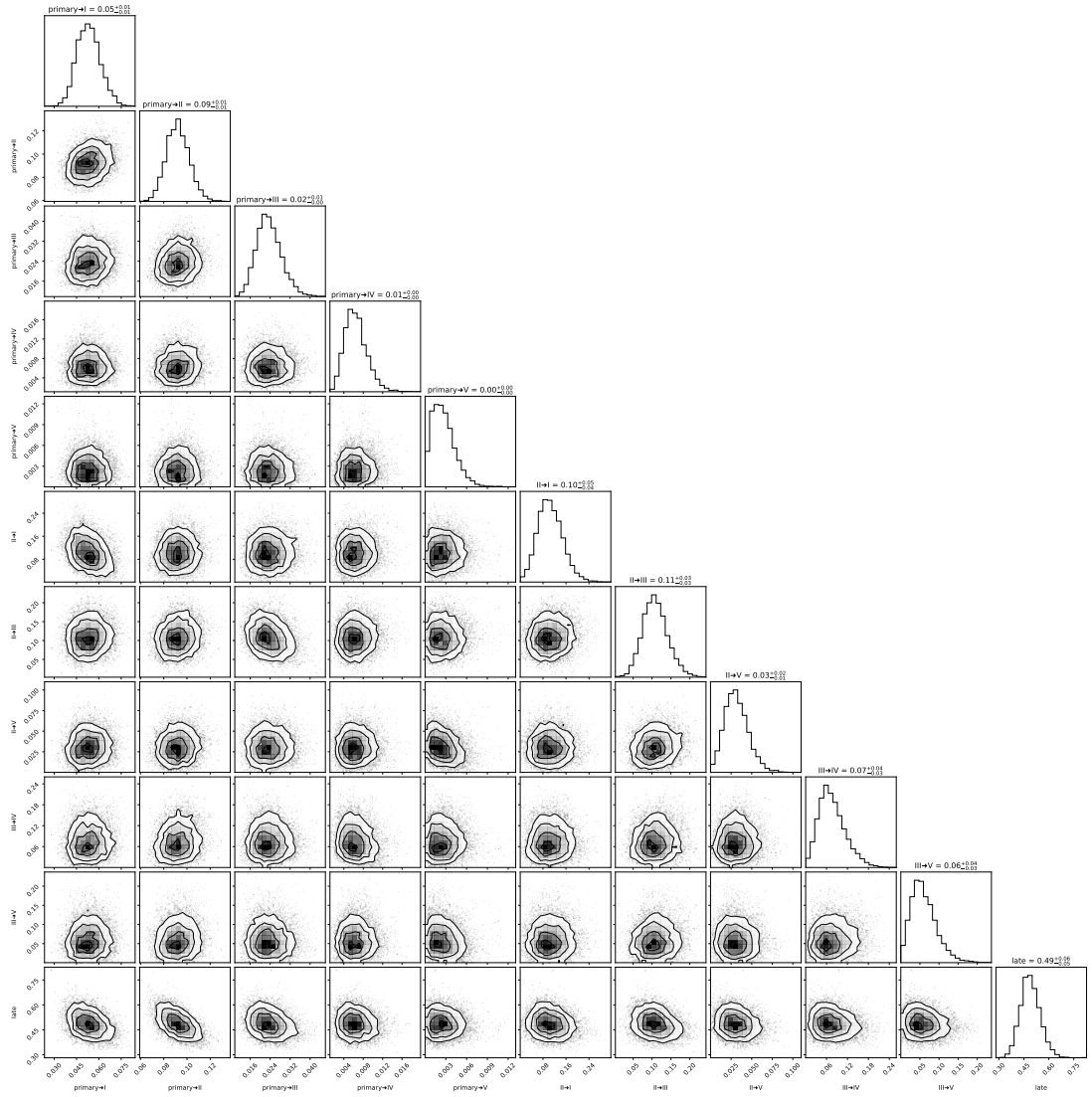

Figure 3.3: Corner plot of the sampled parameters with the 1D (histograms) and 2D marginals (isolines).

In figure 3.4 the distributions of these predicted prevalences are shown for the individual lymph node levels I to IV and the N0 state by the histograms. This means that they

show the predicted percentage of patients that has involvement in the specified level independent of the prediction for all other levels. The N0 histogram represents the percentage of patients with no nodal involvement at all. The results are marginalized over the T-category, so the model predicts a total prevalence for the combined cohort of late and early T-category patients. The solid lines show the beta-posterior distribution

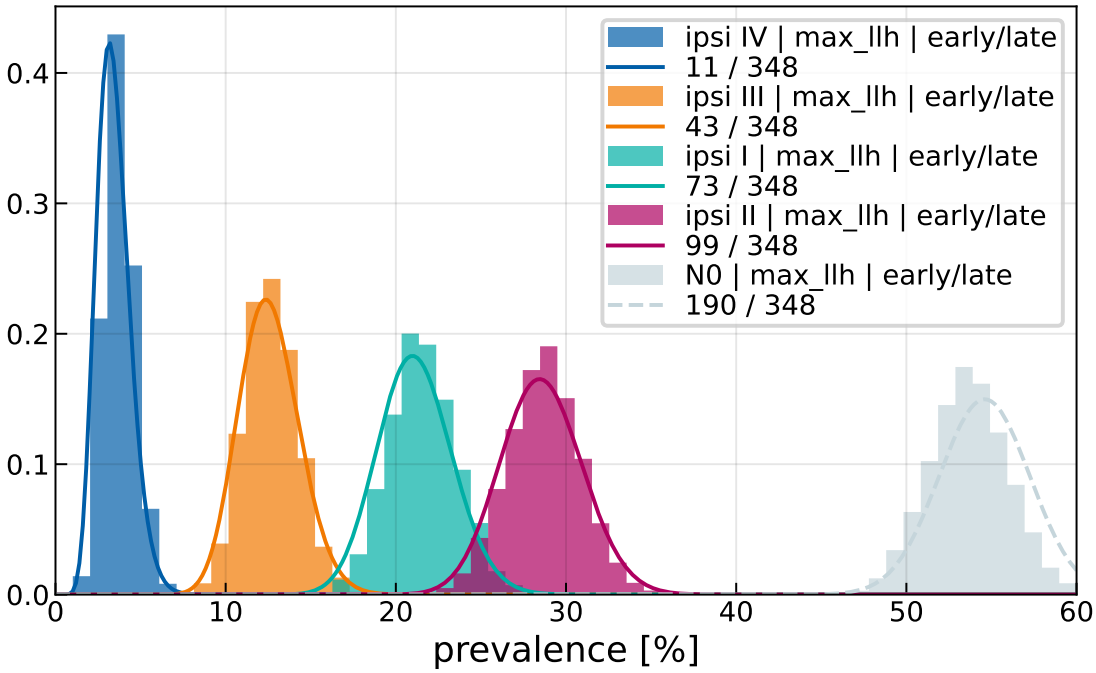

Figure 3.4: Predicted and observed prevalences for the individual lymph node levels and the N0 staging. The histograms show the model predictions while the solid lines show the beta posterior of the observed data.

of the the prevalences observed in the dataset. One can see that the model is able to predict the prevalence for all shown scenarios accurately as the peak of the histograms and their width align with the distribution of the observed prevalences. In the legend the number of patients out of 348 with the specified involvement can be seen. The predicted prevalences are around 21%, 28%, 12%, 3% and 55% respectively for level I to IV and N0.

The same predictions can also be made for the prevalence of specific involvement patterns. This means we can predict the percentage of patients that for example exactly have involvement in LNL I and II but no involvement in level III on the ipsilateral side. Three possible scenarios, again marginalized over T-category, can be seen in figure 3.5. For ipsilateral level I, II and III involved we predict around 3% with this diagnosis, while

for involvement of level II and III but not in level I the prevalence is calculated to be around 4%. For level I and II but not level III involved the prediction is 6%. Again, the predictions of the hidden Markov model fit the observed prevalences well, which shows that also specific involvement patterns and patient's evolutions can be modelled precisely. This is of great value since the risk predictions in the next section are based on specific clinical diagnoses for the lymph node involvement on the ipsilateral side of the patient.

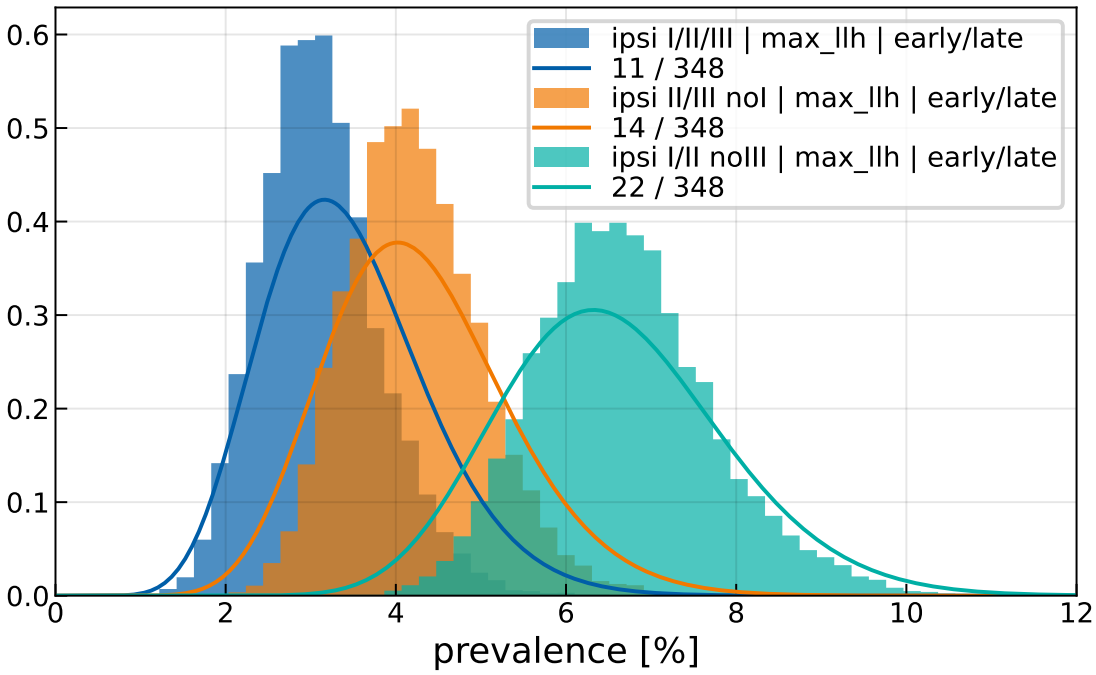

Figure 3.5: Predicted and observed prevalences for a selection of involvement patterns in level I-III. The histograms show the model predictions while the solid lines show the beta posterior of the observed data.

In figure 3.6 the prevalences for the same involvement patterns as in figure 3.5 are shown but in this case the prevalence is stratified for the T-categories early (T1/T2) and late (T3/T4). This stratification is possible due to the time priors and the sampled parameter for the late T-category. As previously shown, the model predictions for the overall patient cohort are very precise. Stratified for T-category, the model can still give a good estimate but in some cases also over- (3.6 (b)) or underestimates (3.6 (c)) the difference in the prevalence between early and late T-category. However, the deviations are usually relatively low and can be explained by the fact that there is only one parameter trained to account for the difference in diagnose times. Introducing

for example level specific time priors would increase the complexity of the model and could lead to overfitting. A possibility would be to not only include T-category as a criteria for the diagnose times and time prior but also the progress of the lymph node involvement. These mentioned limitations have to be kept in mind when doing risk predictions stratified for T-category.

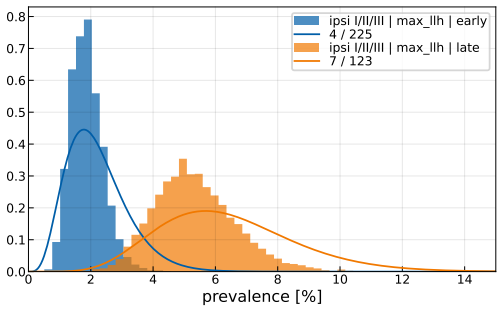

(a) Correctly estimated difference in prevalence between early and late T-category patients

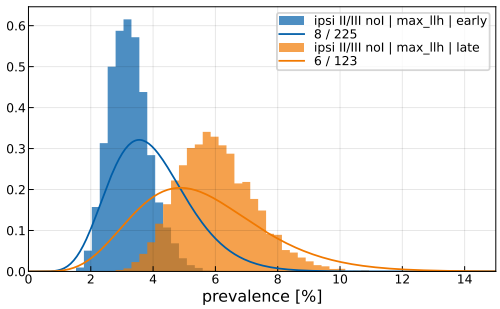

(b) Overestimated difference in prevalence between early and late T-category patients

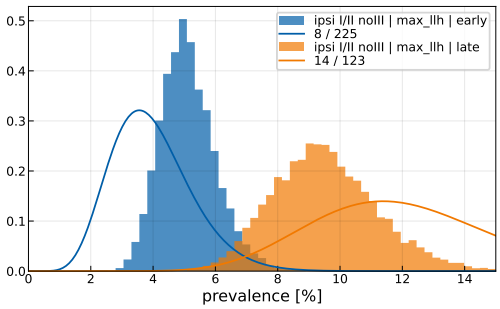

(c) Underestimated difference in prevalence between early and late T-category patients

Figure 3.6: Predicted prevalences for various patterns on the ipsilateral side stratified for T-category early (T1/T2) and late (T3/T4).

3.2.3 Risk assessment of microscopic involvement

The goal of the risk assessment is to predict the probability that a new patient with a given clinical diagnosis $\boldsymbol{z}$ has microscopic and hence not detectable lymph node metastases in a LNL. This risk for a LNL v can be written as followed using Bayes' law:

$$\begin{aligned} R\left(X_v = 1 \mid \mathbf{z}, \hat{\theta}\right) &= \frac{P\left(\mathbf{Z} = \mathbf{z} \mid X_v = 1, \hat{\theta}\right) P\left(X_v = 1 \mid \hat{\theta}\right)}{P(\mathbf{Z} = \mathbf{z} \mid \hat{\theta})} \\ &= \sum_{i:\xi_{iv}=1} \frac{P\left(\mathbf{Z} = \mathbf{z} \mid \boldsymbol{\xi}_i, \hat{\theta}\right) P\left(\boldsymbol{\xi}_i \mid \hat{\theta}\right)}{P(\mathbf{Z} = \mathbf{z} \mid \hat{\theta})} \end{aligned} \tag{3.19}$$

Again, we have a parameter set $\hat{\theta} = \left(\left\{\tilde{b}_v\right\}, \left\{\tilde{t}_{rv}\right\}_{r\in \mathrm{pa}(v)}\right) \forall v \leq V$, representing the probability rates in our graph. The denominator can be calculated using eq. 3.14 for just one T-category and patient. $\boldsymbol{\xi}_i$ are all hidden states that that have LNL v involved. We therefore write ξ_{iv} for the state of LNL v in the state $\boldsymbol{\xi}_i$.

In the computational risk prediction that is used in the next section for the results, a large number of parameter sets $\hat{\boldsymbol{\theta}}$ is drawn using Markov chain Monte Carlo (MCMC). This allows us to approximate the real probability density of the respective risk, also providing uncertainties.

Compared to the prevalence prediction, the risk prediction has the advantage that not only the risk for the general patient cohort is quantified but one can specify the risk based on the clinical diagnosis, which can have a big influence on the probability of metastases in a lymph node level. For example a clinically N0 neck can be expected to have a much lower risk of occult disease in a lymph node level compared to a patient that has clinically diagnosed metastases in neighboring LNLs. However, current guidelines only consider the prevalence in the lymph node levels or even advocate the long-standing convention to irradiate a majority of HNSCC on both sides of the neck and include at least LNL I-III [39, 40]. In the next section we first quantify the risk of occult disease in the levels on the ipsilateral side for different clinical diagnoses and question clinical practice if treatement of level I-III is needed in every case.

Risk of occult disease in level III

Following eq. 3.19, we can now determine the risk for occult metastases in LNL III for different clinical diagnoses based on the sensitivity and specificity of CT imaging (s_N=81%, s_P=76%) according to Pouymayou et al. [12]. The risk of occult disease in LNL III is the most interesting one due to the lower prevalence of metastases in

the pathological evaluation. So the probability to allow exclusion of LNL III from the Clinical Target Volume (CTV) in the case of certain clinical diagnoses is higher compared to level I and II.

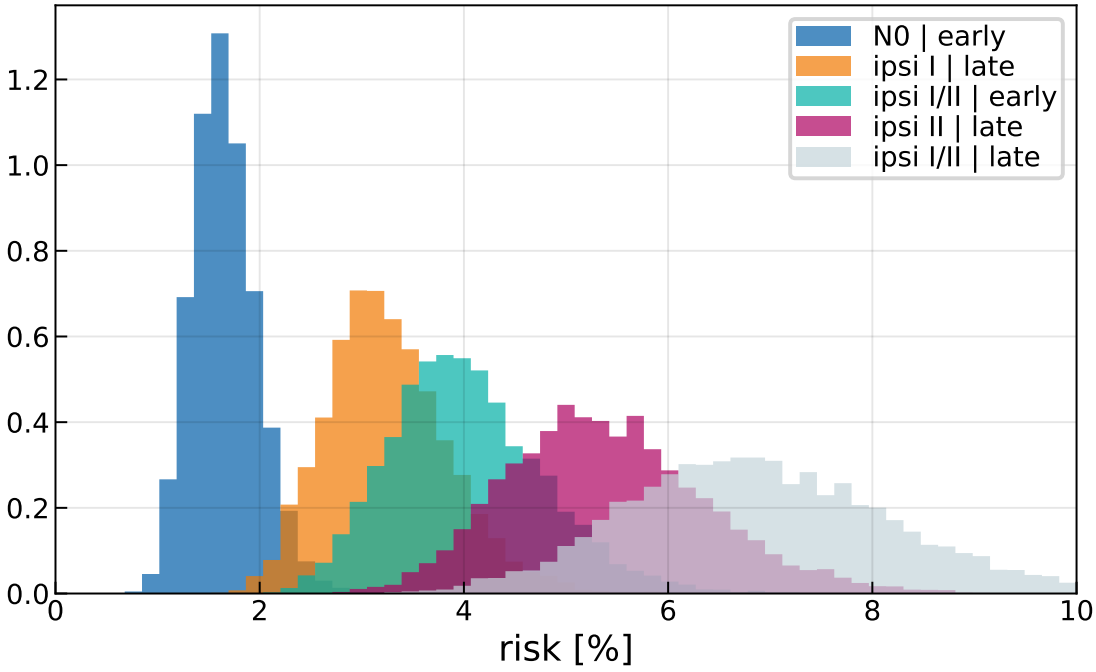

Figure 3.7: Predicted risks of occult disease in level III for a selection of involvement patterns in level I-III (clinical diagnoses). The histograms show the model predictions while the solid lines show the beta posterior of the observed data.

In figure 3.7 one can see the risk of occult disease in LNL III for various scenarios. This means that in the clinical diagnosis no metastases were found in level III and we quantify the risk that there are some microscopic metastases, which were not deteced by the imaging modalities, given a specific clinical diagnosis. Namely, we see for example the risk given a N0, early T-category diagnosis, which is predicted to be around 1.5% with a narrow confidence interval. Also for a clinical diagnosed involvement of ipsilateral level I or II and early T-category patients with level I and II involved, the predicted risk is at 5% or below. Only for late T-category patients with level I and II involved the risk is higher than 5% with approximately 7%. So if we say a threshold and residual risk of 5% would be clinically acceptable, one could leave out treatement of LNL III in the mentioned cases. This would be differ from the current guidelines and support a less aggressive treatement of ipsilateral level III.

Risk of occult disease in level II

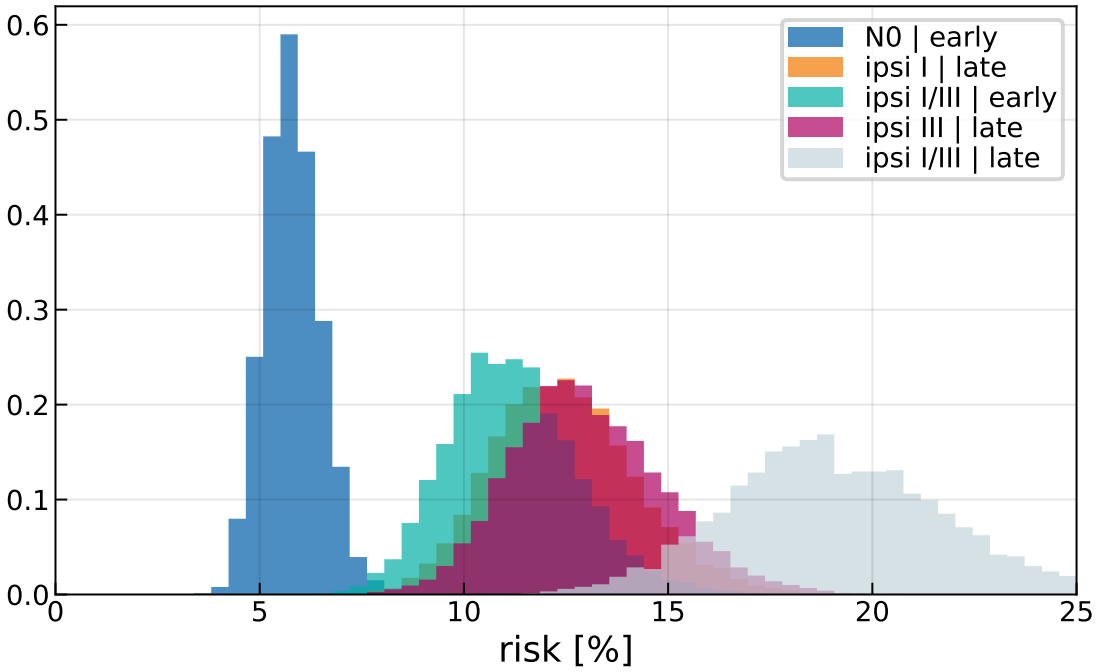

Figure 3.8: Predicted risks of occult disease in level II for a selection of involvement patterns in level I-III (clinical diagnoses). The histograms show the model predictions while the solid lines show the beta posterior of the observed data.

In level II the predicted risks for microscopic metastases are higher than in level III when no or the neighboring levels are involved. This was expected to the way higher observed prevalence of involvement in level II compared to level III. Even in the case of a clinical N0 diagnosis, the risk of microscopic metastases in level II is already slightly higher than the discussed threshold of 5%. Given involvement of adjacent levels, the risk is already at 10% and above and reaches 20% for late T-category patients with level I and III involved. However, it shows that the model can predict the expected high risk scenarios based on the involvement and T-category.

Risk of occult disease in level I

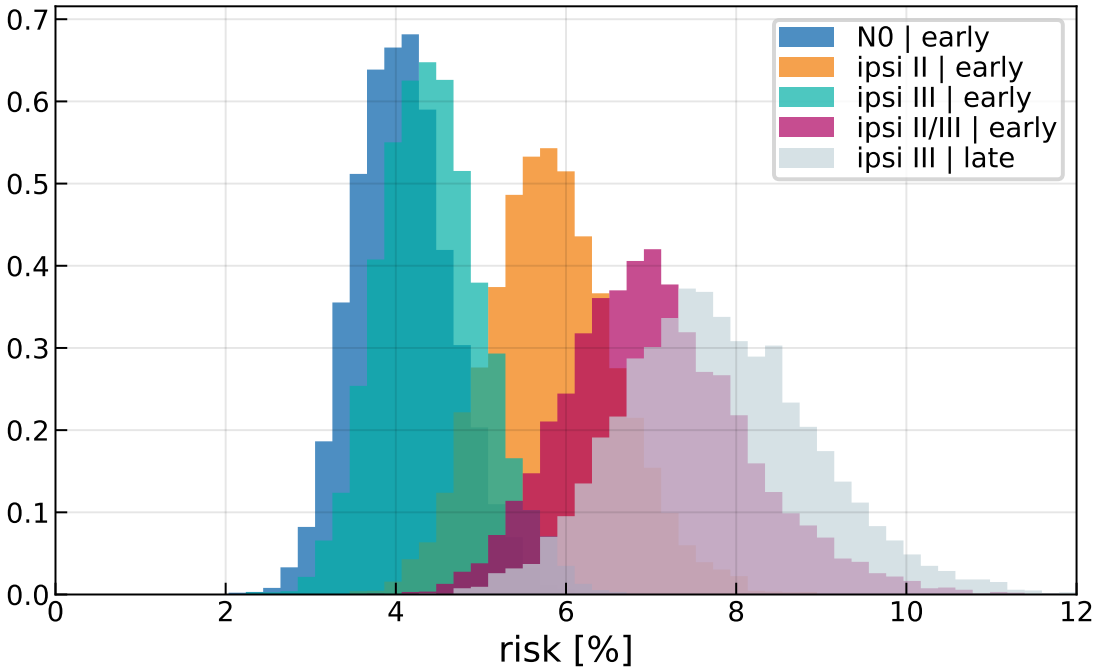

Figure 3.9: Predicted risks of occult disease in level I for a selection of involvement patterns in level I-III (clinical diagnoses). The histograms show the model predictions while the solid lines show the beta posterior of the observed data.

For LNL I we have a similar scenario. As soon as a late T-category tumor or level II is clinically diagnosed, the risk is above the set threshold of 5%. Only in the case of a N0 clinical diagnosis or only involvement of level III combined with an early T-category, the risk is below the threshold at around 4%. Not irradiating level I in the case of clinical involvement in level III or also an N0 diagnosis would be a radical step towards volume de-escalation since level I is currently always treated [41]. However, the availability of pathological data in almost all patients here that represents the ground truth, makes the risk predictions more credible and less prone to underestimations. This could be the case when the model is trained with a sensitivity and specificity of 1 but mainly based on imaging data and therefore clinical diagnoses.

In the next chapter, also the contralateral risks and the influence of midline extension and advanced ipsilateral involvement will be analyzed and discussed together with the here presented ipsilateral risks.

Chapter 4

Bilateral model including midline extension

4.1 Mathematical description

In this chapter, we will extend our previously described model to the contralateral neck. The formalism and model described in chapter 3.1 only deals with one side of the neck, the ipsilateral side where the primary tumor is located. However, metastatic spread to the contralateral side of the neck also occurs depending on the tumor's location and lateralization [13]. So this spread on the contralateral side has to be included in the model. Recent studies have shown that treatment could be limited to the ipsilateral side for many patients [11, 42], however in current clinical practice, a bilateral irradiation or neck dissection is still recommended in most cases [43]. The extension of the hidden Markov model to the contralateral neck could support the selection of patients that are suitable for reduced or even no contralateral neck irradiation.

As previously shown, the involvement on the contralateral side is much lower than on the ipsilateral side. However, the contralateral involvement is not independent of the ipsilateral involvement and the lateralization of the primary tumor. The incidence of contralateral metastases is significantly higher for more advanced ipsilateral involvement and patients where the primary tumor extends over the midline. Therefore, the base probability rates b_v^c for the contralateral side that are expected to be lower than the ipsilateral rates and their dependence on the ipsilateral involvement and midline extension of the primary tumor has to be incorporated into the model.

The new joint conditional probability of the ipsilateral and contralateral side can be written the following way:

$$P\left(\mathbf{X}^{\mathrm{i}}, \mathbf{X}^{\mathrm{c}} \mid \mathbf{Z}^{\mathrm{i}}, \mathbf{Z}^{\mathrm{c}}\right) = \frac{P\left(\mathbf{Z}^{\mathrm{i}}, \mathbf{Z}^{\mathrm{c}} \mid \mathbf{X}^{\mathrm{i}}, \mathbf{X}^{\mathrm{c}}\right) \cdot P\left(\mathbf{X}^{\mathrm{i}}, \mathbf{X}^{\mathrm{c}}\right)}{P\left(\mathbf{Z}^{\mathrm{i}}, \mathbf{Z}^{\mathrm{c}}\right)} \tag{4.1}$$

where the superscripts i and c indicate the ipsilateral and contralateral side. Since the likelihood directly can be factorized, we can rewrite eq. 4.1 the following way:

$$P\left(\mathbf{X}^{\mathrm{i}}, \mathbf{X}^{\mathrm{c}} \mid \mathbf{Z}^{\mathrm{i}}, \mathbf{Z}^{\mathrm{c}}\right) = \frac{P\left(\mathbf{Z}^{\mathrm{i}} \mid \mathbf{X}^{\mathrm{i}}\right) \cdot P\left(\mathbf{Z}^{\mathrm{c}} \mid \mathbf{X}^{\mathrm{c}}\right) \cdot P\left(\mathbf{X}^{\mathrm{i}}, \mathbf{X}^{\mathrm{c}}\right)}{P\left(\mathbf{Z}^{\mathrm{i}}, \mathbf{Z}^{\mathrm{c}}\right)} \tag{4.2}$$

This means that given the true but hidden states of involvement in both sides of the neck, the respective clinical diagnoses are independent. As introduced in eq. 3.12, $P\left(\mathbf{Z}^{\mathrm{i}} \mid \mathbf{X}^{\mathrm{i}}\right)$ and $P\left(\mathbf{Z}^{\mathrm{c}} \mid \mathbf{X}^{\mathrm{c}}\right)$ are given by the observation matrices $\mathbf{B}^{\mathrm{i}}$ and $\mathbf{B}^{\mathrm{c}}$.

To describe the joint probability of the hidden states $P\left(\mathbf{X}^{\mathrm{i}}, \mathbf{X}^{\mathrm{c}}\right)$, we assume that there is no direct spread between ipsilateral and contralateral LNLs. This means that the only arcs to the contralateral LNLs originate from the primary tumor, modelling the origin of the contralateral spread. Therefore, the only correlation of the probability for involvement of the ipsilateral and contralateral side is via the diagnose time t. This means we can write the joint probability as a sum over the time-steps, again including the time prior for the diagnose times.

$$\begin{aligned} P\left(\mathbf{X}^{\mathrm{i}}, \mathbf{X}^{\mathrm{c}}\right) &= \sum_{t \in T} p(t) \cdot P\left(\mathbf{X}^{\mathrm{i}}, \mathbf{X}^{\mathrm{c}} \mid t\right) \\ &= \sum_{t \in T} p(t) \cdot P\left(\mathbf{X}^{\mathrm{c}} \mid t\right) \cdot P^{\top}\left(\mathbf{X}^{\mathrm{i}} \mid t\right) \end{aligned} \tag{4.3}$$

Using the notation from chapter 3.1 and

$$\boldsymbol{\Lambda} := P(\mathbf{X} \mid \mathbf{t}) = \begin{pmatrix} \boldsymbol{\pi}^{\top} \cdot (\mathbf{A})^{0} \\ \boldsymbol{\pi}^{\top} \cdot (\mathbf{A})^{1} \\ \vdots \\ \boldsymbol{\pi}^{\top} \cdot (\mathbf{A})^{t_{\max}} \end{pmatrix} \tag{4.4}$$

we can write $P\left(\mathbf{X}^{\mathrm{i}}, \mathbf{X}^{\mathrm{c}}\right)$ for the specific states $\mathbf{X}^{\mathrm{c}} = \boldsymbol{\xi}_{\mathrm{n}}$ and $\mathbf{X}^{\mathrm{i}} = \boldsymbol{\xi}_{\mathrm{m}}$ as followed:

$$P\left(\mathbf{X}^{\mathrm{c}} = \boldsymbol{\xi}_n, \mathbf{X}^{\mathrm{i}} = \boldsymbol{\xi}_m\right) = \left[\boldsymbol{\Lambda}_{\mathrm{c}}^{\top} \cdot \operatorname{diag} p(\mathbf{t}) \cdot \boldsymbol{\Lambda}_{\mathrm{i}}\right]_{n,m} \tag{4.5}$$

The rown n and column m are taken to find the exact probability of being in the given state.

Taking equation 4.5 and following the same principle as in 3.13 by multiplying the observation matrices $\mathbf{B}$ onto both sides, we get:

$$P\left(\mathbf{Z}^{\mathrm{c}} = \boldsymbol{\zeta}_n, \mathbf{Z}^{\mathrm{i}} = \boldsymbol{\zeta}_m\right) = \left[\mathbf{B}^{\top} \cdot \boldsymbol{\Lambda}_{\mathrm{c}}^{\top} \cdot \operatorname{diag} p(\mathbf{t}) \cdot \boldsymbol{\Lambda}_{\mathrm{i}} \cdot \mathbf{B}\right]_{n,m} \tag{4.6}$$

Based on eq. 4.5 and 4.6 we do now have all necessary terms to perform the parameter inference and the risk prediction (introduced in eq. 3.14 and eq. respectively 3.19) also for the bilateral case. The likelihood function is then defined followingly:

$$P(\boldsymbol{\mathcal{Z}} \mid \theta) = \prod_{T=1}^{T_{max}} \left[\mathbf{B}^{\top} \cdot \boldsymbol{\Lambda}_{\mathrm{c}}^{\top} \cdot \operatorname{diag} p_T(\mathbf{t}) \cdot \boldsymbol{\Lambda}_{\mathrm{i}} \cdot \mathbf{B}\right] \cdot \boldsymbol{f}_T \tag{4.7}$$

The model parameters θ are now divided into θ^{i} and θ^{c}, as both sides now have their own set of spread probabilites that are used to parametrize the transition matrices $\mathbf{A}^{\mathrm{i}}$ and $\mathbf{A}^{\mathrm{c}}$.

As already mentioned, the spread probabilites from the primary tumor for the ipsilateral and contralateral side (b^{i} and b^{c}) are assumed to be different. However, the spread probabilites among the LNLs should be equal based on the assumption that the lymphatic network in the head and neck region is symmetric. This still does not allow us to account for a higher involvement on the contralateral side when the tumor crosses the midline as it has been shown in the table 2.5. Therefore, we introduce two sets of spread probabilites from the primary tumor to the LNLs on the contralateral side:

- $b_v^{\mathrm{c},\mathrm{e}}$: Contralateral spread probabilities when the primary tumor extends over the mid-sagittal plane.
- $b_v^{\mathrm{c},\not{\mathrm{e}}}$: Contralateral spread probabilities when the primary tumor extends over the mid-sagittal plane.

The assumption we make is, that a linear mixing parameter α can define the contralateral spread from the primary tumor to the LNLs as a linear superposition between the ipsilateral spread parameters, which represents the maximum, and the contralateral spread probabilites for tumors without midline extension, which represents the minimum:

$$b_v^{\mathrm{c},\mathrm{e}} = \alpha \cdot b_v^{\mathrm{i}} + (1 - \alpha) \cdot b_v^{\mathrm{c},\not{\mathrm{e}}} \tag{4.8}$$

This mixing parameter is a new model parameter and must be inferred from the data. It comes with the strong assumption that the base probability rates from the primary tumor to the contralateral side follow the same linear increase for all LNLs when the tumor crosses the midline. Although this assumption is probably not strictly true, it helps to account for differences in the involvement patterns on the contralateral side

between tumors with and without midline extension by adding just one parameter to the model. By adding this midline extension information, we now have an update likelihood function accounting for the changed base spread probabilities:

$$P(\boldsymbol{\mathcal{Z}} \mid \theta) = \prod_{m \in \{e, \not{e}\}} \left[\prod_{T=1}^{T_{max}} \left[\mathbf{B}^{\top} \cdot \mathbf{\Lambda}_{\mathrm{c,m}}^{\top} \cdot \operatorname{diag} p_T(\mathbf{t}) \cdot \mathbf{\Lambda}_{\mathrm{i}} \cdot \mathbf{B} \right] \cdot \boldsymbol{f}_{T,m} \right] \tag{4.9}$$

where $m = 0$ represents tumors without midline extension and $m = 1$ tumors with midline extension. Since the contralateral transition matrix changes is dependent on the spread probabilities, we now have a dependence on the midline extension in the matrix $\mathbf{\Lambda}_c$.

A challenge we face for the OCSCC dataset from Lyon is, that we do not have any midline extension information available. So we can not simply apply the likelihood function described in eq. 4.9 as we have to incorporate an approach for patients without available midline extension information. In the following two sections we will discuss and describe the two approaches to account for this missing information. Later, both model extensions will be tested with the real datasets.

4.2 Model extensions

4.2.1 Marginalization over midline extension states

The idea of marginalizing over the midline extension states includes a new parameter inferred from the data. This parameter is the probability of a patient to have a primary tumor that extends over the mid-sagittal plane $P(m = 1)$. For patients with known midline extension state, either the part of the likelihood accounting for midline extension or the part accounting for no midline extension is calculated. For patients with no information about the midline extension both parts are calculated. To then marginalized over the midline extension state, the separate parts of the likelihood function have to be weighted by the probability of midline extension or no midline extension and the number of the corresponding patients. We can write the likelihood in the following way to show the different contributions of the three possible patient cohorts (midline extension: $N_{m=1}$, no midline extension: $N_{m=0}$ and unknown midline extension: $N_{m=?}$):

$$
\begin{aligned}
&P(m=1)^{N_e} \cdot \prod_{i=1}^{N_e} \sum_{\mathbf{X}} P(\mathbf{Z}_i \mid \mathbf{X}) P\left(\mathbf{X} \mid \theta, m=1\right) \\
&\cdot P(m=0)^{N_{\not e}} \cdot \prod_{i=1}^{N_{\not e}} \sum_{\mathbf{X}} P(\mathbf{Z}_i \mid \mathbf{X}) P\left(\mathbf{X} \mid \theta, m=0\right) \\
&\cdot \prod_{i=1}^{N_?} \Bigg[P(m=1) \sum_{\mathbf{X}} P(\mathbf{Z}_i \mid \mathbf{X}) P\left(\mathbf{X} \mid \theta, m=1\right) \\
&+ P(m=0) \sum_{\mathbf{X}} P(\mathbf{Z}_i \mid \mathbf{X}) P\left(\mathbf{X} \mid \theta, m=0\right) \Bigg]
\end{aligned}
\tag{4.10}
$$

For the patient cohorts with known midline extension, the log-likelihood can be easily obtained by taking the logarithm of the sum of all hidden states and summing over all patients in this cohort. However, for the patient cohort with unknown midline extension ($N_?$)this can not be done so easily for the two contributions (midline extension, no midline extension) and the logarithm of the whole contribution of a patient has to be taken.

This is the first approach and a possible solution to include also patients without midline extension information and still include their valuable information about the pathological involvement in the LNLs on the ipsilateral and contralateral side. The model predictions are shown and analyzed in section 4.3.1.

4.2.2 Time evolution of midline extension states

The limitation of the approach presented in the previous section is the time independence of the midline extension state. In the case of a tumor extending the midline it only holds the information that there was a midline extension at the point of diagnosis. However, it does not consider the patient's evolution over time. The following method accounts for that evoultion of the midline extension and tracks the probability of the midline extension state at every time step. This generalizes the approach to include the midline extension information into the hidden Markov model and can at the same time deal with missing information as it is the case in the CLB dataset.

A possibility would be to just add the midline extension information to the existing transition matrix $\mathbf{A}$. However this would lead to double the number of states since every existing state for the possible combinations of lymph node involvement would then be represented twice. Once with midline extension and once without midline extension. This would increase the number of entries in the transition matrix from 2^{2V}, V being

the number of included lymph node levels, to $2^{2(V+1)}$ and hence increase the size by a factor of 4. As a result, the training time of the model would be significantly increased. Therefore it makes sense to track the midline state on its own since it can be separated quite easily. We are going to show this newly introduced formalism in this section.

To track the midline extension state, we need the same tools as for the lymph node involvement. Therefore, we introduce a midline state vector that represents the probabilites for the midline extension states at a certain time-step t:

$$\boldsymbol{\omega}[t] = \begin{bmatrix} P\left(m = 0 \mid t\right) \\ P\left(m = 1 \mid t\right) \end{bmatrix} \tag{4.11}$$

Additionally, we need a transition matrix for the midline extension state to evolve the state vector $\boldsymbol{\omega}$ over the time.

$$\mathbf{A}_M = \begin{bmatrix} P\left(m[t+1] = 0 \mid m[t] = 0\right) & P\left(m[t+1] = 1 \mid m[t] = 0\right) \\ 0 & 1 \end{bmatrix} \tag{4.12}$$

We can call the probability $P\left(m[t+1] = 1 \mid m[t] = 0\right)$ the midline extension probability rate. It describes the probability that a tumor has a midline extension from one timestep to the next one. This midline extension transition rate is the only additional model parameter that has to be sampled and therefore this model extension comes with a low cost but also introduces a more precise way to model the true state of the midline extension at any time point. The diagnose matrix that contains the probabilities to see the provided diagnosis, given any possible hidden state, is defined separately for the midline extension state and the lymph node involvement. The diagnose matrix for the midline extension $\mathbf{D}_{M,T}$ is defined as:

$$\mathbf{D}_{M,T} = \begin{bmatrix} 1 - m_1 & \dots & 1 - m_N \\ m_1 & \dots & m_N \end{bmatrix} \tag{4.13}$$

Where T stands for the respective T-category and m_i is the midline extension state of patient i out of N patients. $m_i = 0$ means that patient i has no midline extension while $m_j = 1$ means that patient j has midline extension. If the midline extension is unknown for a patient k, $1 - m_k$ and m_k are set to 1 since we have no additional information tending to one or the other state. The diagnose matrix for the ipsilateral side $\mathbf{D}_{T,i}$ and the contralateral side $\mathbf{D}_{T,c}$ follow the same principle where the most likely state is set to one. The number of columns of the matrix therefore is the same and corresponding to the number of patients. The number of rows is not just two as for the midline extension diagnose matrix but 2^V, since this is the possible number of states for V LNLs. The most likely state is determined by the maximum likelihood

consensus diagnosis method described in chapter 4 of [13].

Due to the fact that the midline extension can occur in every timestep, the total probability of a midline extension up to a certain timestep is not constant. Therefore we have to evolve the state vectors recursively over time. We have our midline extension state vector $\boldsymbol{\omega}[t]$ that evolves simply with the midline extension transition matrix:

$$\boldsymbol{\omega}[t+1] = \boldsymbol{\omega}[t] \cdot \mathbf{A}_M \tag{4.14}$$

For the state vector containing the state probabilities given without midline extension of the tumor, it is again a simple multiplication with the transition matrix $\mathbf{A}_{m=0}$. However, for state vector considering midline extension of the tumor, we need a linear combination with the entries of the midline extenstion state vector as weights:

$$\begin{aligned} \boldsymbol{\varphi}_{\not e}[t+1] &= \boldsymbol{\varphi}_{\not e}[t] \cdot \mathbf{A}_{\not e} \\ \boldsymbol{\varphi}_{e}[t+1] &= \boldsymbol{\omega}_1[t] \cdot \boldsymbol{\varphi}_{\not e}[t+1] + \boldsymbol{\omega}_2[t] \cdot \boldsymbol{\varphi}_{e}[t] \cdot \mathbf{A}_{e} \end{aligned} \tag{4.15}$$

where $\boldsymbol{\omega}_1$ denotes the first entry of the midline extension state vector (no midline extension) and $\boldsymbol{\omega}_2$ the second entry (midline extension). $\boldsymbol{\varphi}_{\not e}[t+1]$ and $\boldsymbol{\varphi}_{e}[t+1]$ denote the state vector with the probabilities for all possible states at time point $t+1$ cosidering no midline extension respectively midline extension.

These evolved state vectors can then be written in the form of the matrix $\boldsymbol{\Lambda}$ that was described in 4.4 and are used to define the joint diagnose probabilities of no midline extension ($\mathbf{J}_{\not e}$) and midline extension ($\mathbf{J}_{e}$):

$$\begin{aligned} \mathbf{J}_{T,\not e} &= \sum_k \left[\mathbf{D}_{T,i} \odot \left[\boldsymbol{\Lambda}_{i,\not e}^{\top} \cdot diag(p_T(\mathbf{t})) \cdot \boldsymbol{\Lambda}_{c,\not e}^{\top} \cdot \mathbf{D}_{T,c} \right] \right]_k \\ \mathbf{J}_{T,e} &= \sum_k \left[\mathbf{D}_{T,i} \odot \left[\boldsymbol{\Lambda}_{i,e}^{\top} \cdot diag(p_T(\mathbf{t})) \cdot \boldsymbol{\Lambda}_{c,e}^{\top} \cdot \mathbf{D}_{T,c} \right] \right]_k \end{aligned} \tag{4.16}$$

where T stands for the T-category, k denotes the kth column of the matrix, $\odot$ represents the Hadamard product and i and c stand for the ipsilateral and contralateral side. $\mathbf{D}_{T,c}$ and $\mathbf{D}_{T,i}$ are constructed in the same way as the matrix for the midline extension but do not contain the observed midline extension state. They hold the information of the observed state of lymph node involvement for every individual patient. So the observed state is denoted by a 1 while the other states are represented by a 0.

By combining the two joint diagnose probabilities for midline extension and no midline extension, we can write down the complete **likelihood function** by taking the product over the T-categories:

$$P(\mathcal{Z} \mid \theta) = \prod_{T=1}^{T_{max}} \left[\sum_{l} \left[\mathbf{J}_T \cdot \mathbf{D}_{M,T}^{\top} \right]_l \right] \quad , \quad \mathbf{J}_T = \begin{bmatrix} \mathbf{J}_{T,\not e} \\ \mathbf{J}_{T,e} \end{bmatrix} \tag{4.17}$$

where l again is the lth column of the matrix. With this function, finally the likelihoods of all patients in the combined dataset can be computed when splitted into T-categories corresponding to the different time priors.

4.3 Application to OCSCC

The model assumptions for this section are the same as for the unilateral model described in subsection 3.2.1. However, now not only the data for the ipsilateral side but also all available data for the contralateral side of the neck is included.

4.3.1 Sampled parameters and predicted prevalences

In figure 4.1 and 4.2 the trained model parameters are displayed with the 1D (histograms) and 2D marginals (isolines). Figure 4.1 is based on the model with the simple marginalization over the midline extension as described in section 4.2.1, while figure 4.2 shows the parameters of the model considering the evolution of the midline extension state over time as described in the previous section 4.2.2. As expected, the ipsilateral base parameters are sampled to the same values as with the unilateral model shown in figure 3.3. Also the transmission probabilities between the lymph node levels are very similar to the unilateral model in both bilateral models. This makes sense as no difference in spread between the LNLs should be observed when extending the model to the contralateral side of the neck. The contralateral base parameters are very low, explaining the low prevalence of involvement on the contralateral side and are equivalent for both midline marginalization approaches. So overall both approaches lead to very similar probability rates respectively model parameters as also the diagnose time for late T-category patients is expected to be distributed equally. Minor differences occur for the mixing parameter α but due to the very broad distribution of the parameter in both models (visible in the histogram), no significant difference can be observed.

The most relevant parameter in this case is the midline extension probability, as it was newly added to the model and implement with the two mentioned methods. The different approaches are also the reason for the different values that are trained for this parameter. In the case where we simply marginalize over the midline extension (figure 4.1) an average probability of 0.17 gets sampled. This is the total probability for a patient to have a tumor extending over the midline at the point of diagnosis. This is in agreement with the value observed in the dataset where 16% (33 patients) out of

the 202 patients with known midline extension state have a tumor extending over the mid-saggital plane. Therefore, also a similar or slightly higher percentage of midline extensions is expected for the patient cohort of the CLB dataset, for whom the midline extension state is unknown.

In the approach where we evolve the midline extension state over time, the sampled midline extension parameter is not the probability for a patient to have midline extension at the point of the diagnosis but has to be interpreted analogously to the other parameter as a probability rate. So it is the probability that a midline extension occurs from one time step to the next one. In our case a value of 0.05 gets trained. To calculate the predicted probability that a tumor extends over the midline at the point of diagnosis, we have to marginalize over all time-steps and calculate the product over all possibilities of the diagnose point and time point of the midline extension. We can write that in the following way for a given T-category T:

$$P(m=1) = 1 - \sum_{t=1}^{N} \left(\prod_{i=1}^{t-1} (1 - P\left(m[i] = 1 \mid m[i-1] = 0\right)) \cdot p_T[t] \right) \tag{4.18}$$

where N is the number of time-steps and $p_T[t]$ is the probability for a patient with T-category T to be diagnosed at time-point t. $P\left(m[i] = 1 \mid m[i-1] = 0\right)$ is the probability that a midline extension occurs from the $i-1$th to the ith time-step. In our case this is a constant value and the sampled model parameter mentioned earlier.

In our case we have early and late T-category patients, the two correspoinding binomial distributions as the prior and $P\left(m[i] = 1 \mid m[i-1] = 0\right) = 0.05$. The priors are visualized in figure 3.2 and are mathematically described by:

$$\begin{aligned} \text{early:} &= B(10, 0.30) \\ \text{late:} &= B(10, 0.48) \end{aligned} \tag{4.19}$$

where $B(,)$ denotes the binomial distribution and 10 is the number of time-steps. 0.3 and 0.48 means that, on average, early T-category patients are diagnosed in the third time step and late T-category patients around the fifth time step. As mentioned earlier, the probability for the early T-category is fixed and the value for the late T-category is learned by the model. We can now calculate the probability of a midline extension at the point of diagnosis separately for early and late T-category patients:

$$\begin{aligned} P(m = 1 \mid T = \text{early}) &= 0.140 \\ P(m = 1 \mid T = \text{late}) &= 0.236 \end{aligned} \tag{4.20}$$

These values are in agreement with the values observed in the ISB dataset where 13.3%

(20 out of 150 patients) and 25.0% (13 out of 52 patients) were observed respectively.

So it has been shown that both introduced model extensions can predict the midline extension probability reliably. The approach where the time evolution of the midline extension is incorporated, we have the advantage that it can also predict the probability separately for every T-category that is specified in the model.

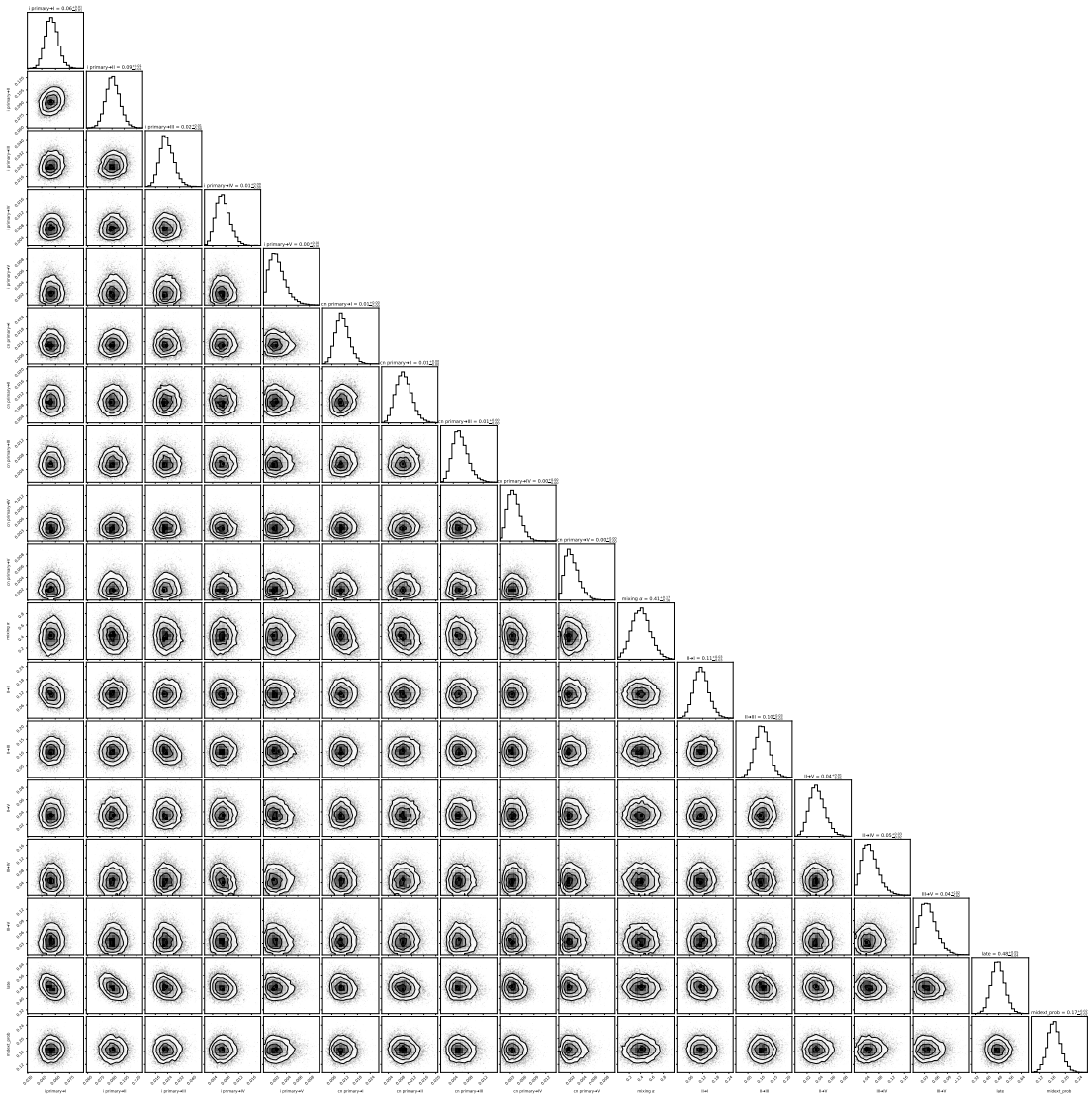

Figure 4.1: Corner plot of the sampled parameters with the 1D (histograms) and 2D marginals (isolines) for the bilateral model including marginalization over the midline extension

This advantage of the midline extension time evolution model could also have a positive effect on the model performance in the prevalence and risk predicition. We will further analyze this in the following sections.

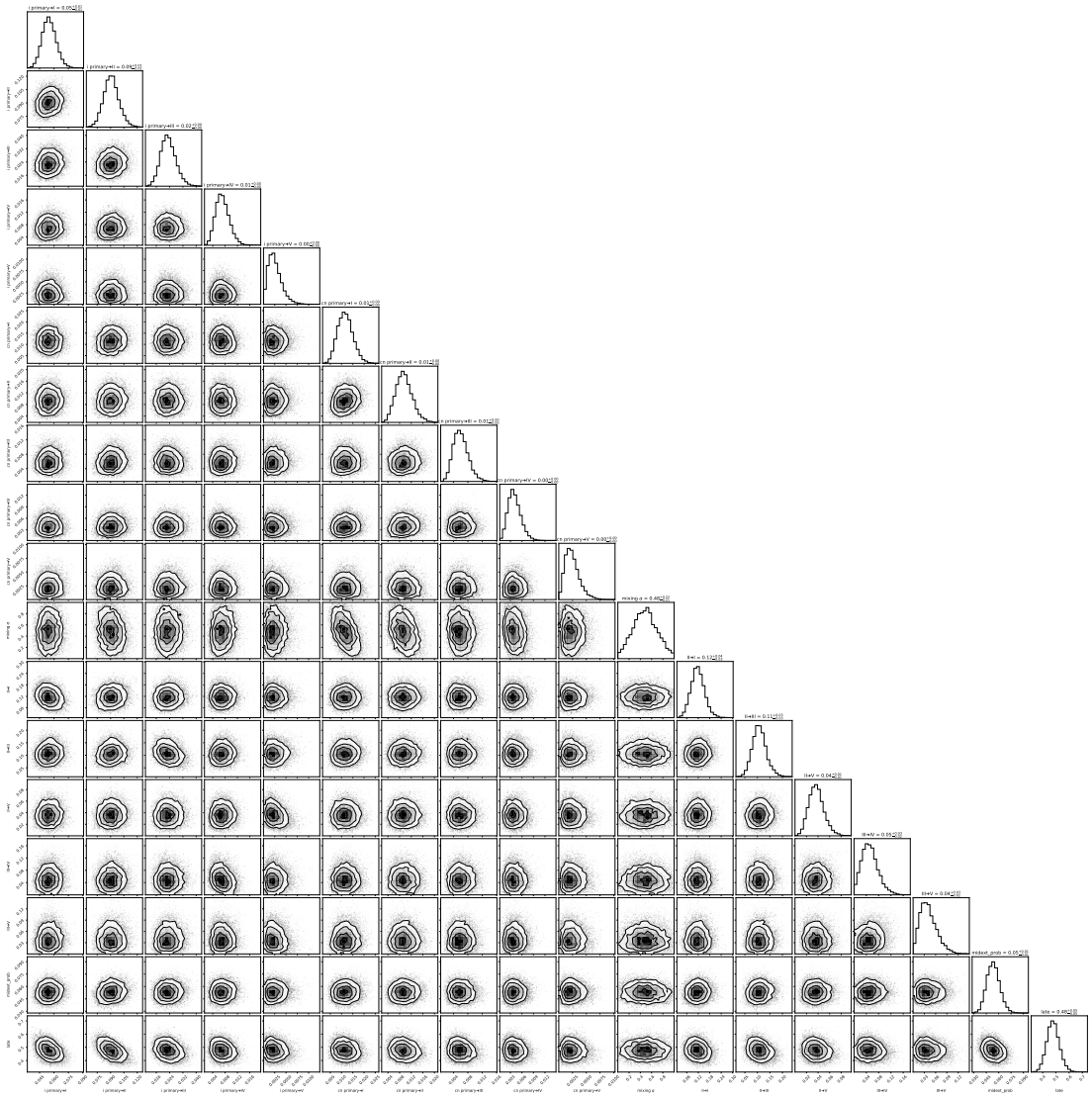

Figure 4.2: Corner plot of the sampled parameters with the 1D (histograms) and 2D marginals (isolines) for the bilateral model including time evolution of the midline extension state

In figure 4.3 the predicted prevalences for all ipsilateral LNLs can be seen in the form

of histograms for both model approaches ((a): marginalization over midline extension, (b): time evolution model). The beta posteriors of the observed prevalences are shown by the solid lines. We have already shown these prevalences predicted by the unilateral model in figure 3.4. Both bilateral models predict the prevalences equal and as good as the unilateral model on the ipsilateral side when not stratified for T-category.

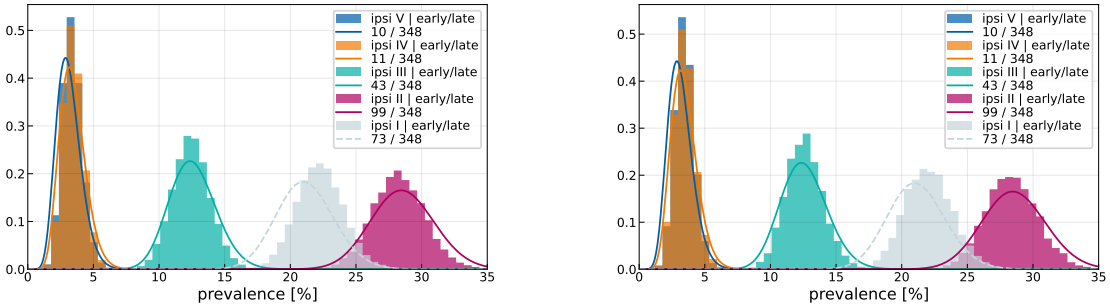

(a) (b)

Figure 4.3: Predicted and observed prevalences for the ipsilateral involvement in the individual LNLs of the model with (a): marginalization over the midline extension and (b): time evolution of the midline extension state.

Looking at figure 4.4 we can see the same comparison and predictions of the bilateral models for the contralateral LNLs. Overall, both models again are able to describe the observed prevalences well but some minor differences arise. While the marginalization model predicts the prevalence in contralateral level II slightly better, the time evolution model is closer to the observed data for level I. This can partially be explained by the higher transmission rate from level II to I in the time evolution model. The other reason could be a minor difference in the spread from the primary tumor to level II.

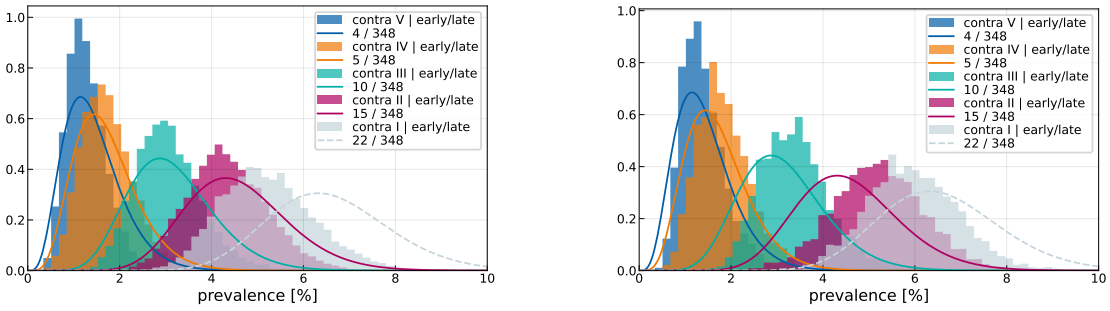

(a) (b)

Figure 4.4: Predicted and obvserved prevalences for the contralateral involvement in the individual LNLs of the model with (a): marginalization over the midline extension and (b): time evolution of the midline extension state.

The prevalence predictions again can not only be made for individual levels but also for specific involvement patterns. The results for both models are displayed in figure 4.5. Three of the four displayed scenarios are described well by both models, also including the contralateral case. However, a deviation is observed for both models when we look at combined involvement of ipsilateral and contralateral level I.

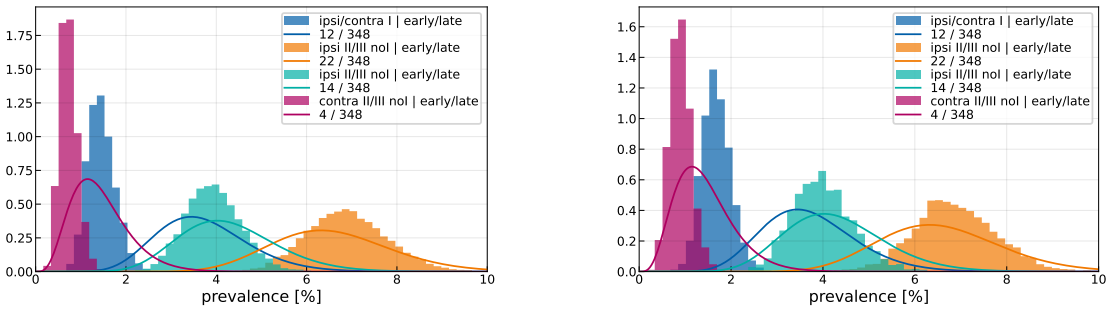

Figure 4.5: Predicted and observed prevalences for various involvement patterns in level I-III (ipsilateral and contralateral) of the model with (a): marginalization over the midline extension and (b): time evolution of the midline extension state.

A possible explanation is that this scenario is very rare and therefore it makes sense that the model puts less attention to it. This can also be observed in figure 4.6. Stratified for T-category in the same scenario, the prevalence for early T-category patients is estimated quite precisely but for late T-category patients it is underestimated by a relatively large margin in both models. So it is not the known case where either the early or late T-category gets underestimated and the other gets overestimated as it is seen for example when ipsilateral level II and III but not I is involved (4.6b, 4.6d). To model it correctly, the sampled parameter for the late T-category would have to be much larger, associating late T-category patients to a much later time of diagnosis. This would lead to larger deviations in many cases with higher prevalence, resulting in a worse value of the likelihood function. So the model has not enough degrees of freedom to correctly describe all these scenarios. Therefore we especially have to be aware of the fact that risks for late T-category patients with contralateral involvement could be underestimated. However, regarding current clinical practice with mostly bilateral treatment, we are mostly interested in the cases where we only have ipsilateral involvement.

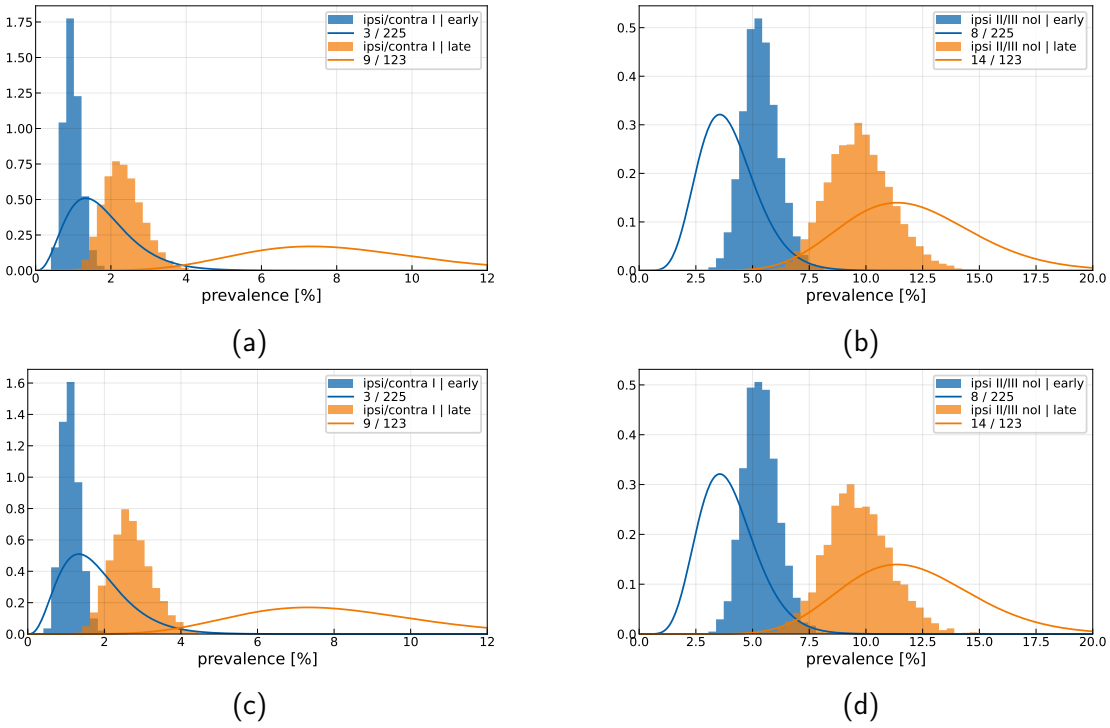

Figure 4.6: Predicted and observed prevalences for two scenarios stratified for T-category of the model with (a,b): marginalization over the midline extension and (c,d): time evolution of the midline extension state.

Another important risk factor is midline extension. So it makes sense to also look at the prevalences for contralateral levels stratified for midline extension. The results for both bilateral models and involvement of contralateral level II can be seen in figure 4.7. One can see that the prevalence in contralateral level II is described well by the model when no midline extension is present. Both bilateral models predict a strong increase for the involvement of contralateral level II when midline extension occurs. These predictions are higher than what is observed in the data. However, it has to be said that in both T-categories there was each only one patient with midline extension. This can also be seen by the very wide posterior of the observed data in these cases. Therefore the discrepancies should not be weighted too strongly and the fact that a clean separation of patients with and without midline extension is possible should be highlighted.

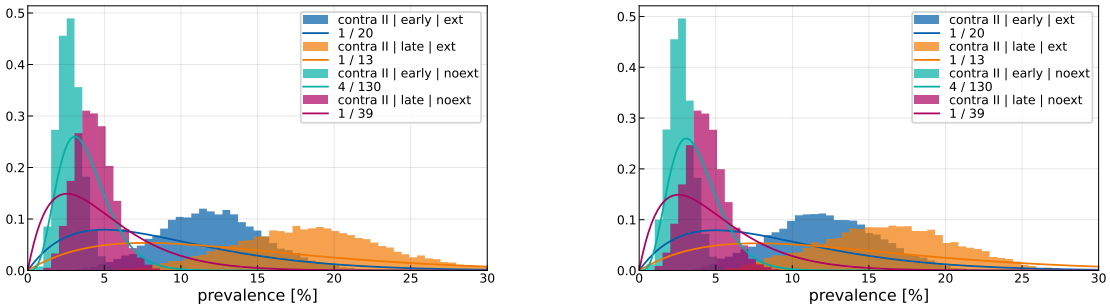

(a) (b)

Figure 4.7: Predicted and observed prevalence in contralateral level II stratified for T-category and midline extension of the model with (a): marginalization over the midline extension and (b): time evolution of the midline extension state.

4.3.2 Risk assessment of microscopic involvement

For the ipsilateral side, as previously mentioned, the two tested bilateral models show almost identical results to the unilateral model discussed in chapter 3. Therefore, we are only going to show and discuss the risks for occult disease in contralateral levels based on the bilateral model including midline extension. From now on, all results are generated by the model considering the time evolution of the midline extension since it follows a more general and sophisticated approach and has shown to be at least equal in performance to the model with simple marginalization over the midline extension.

In figure 4.8 the risks of occult disease in contralateral level I and II are shown for various possible clinical involvements on the ipsilateral side. Cases where only the ipsilateral side shows clinical diagnosed metastases are of most interest since current guidelines suggest bilateral treatment of the neck for at least level I, II and III in every case [39, 40]. So the potential for volume de-escalation of the CTV could be the largest when only ipsilateral levels are clinically involved.

One can see that the risk for occult disease in level I and II on the contralateral side of the neck is very low for all selected involvement patterns on the ipsilateral side. In level I the risk does not increase above 2% even for the very improbable clinical diagnosis of late T-category and involvement of all ipsilateral levels I to V. In contralateral level II the risk even is expected to be below 1% given the same diagnosis. Also to be mentioned is, that the expected risk of microscopic metastasis on the contralateral side does only marginally increase with advanced ipsilateral involvement and also the influence of the T-category is insignificant. Therefore, assuming a clinically relevant threshold risk of 5%, unilateral treatment of the neck could be a possibility when the

clinical diagnosis only includes ipsilateral involvement of the LNLs.

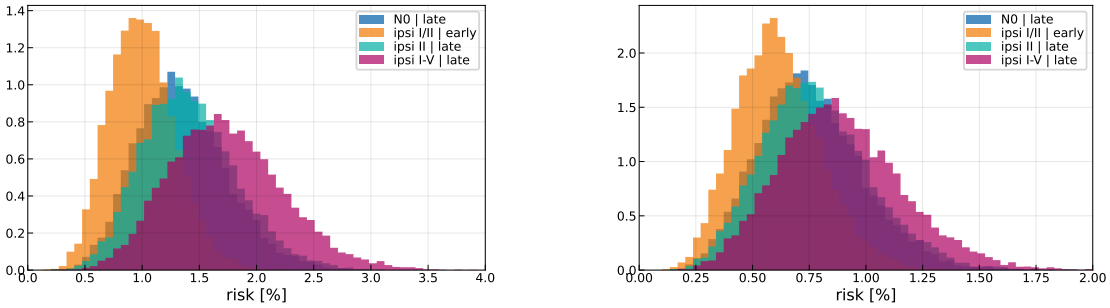

(a) (b)

Figure 4.8: Histogram showing the risk of occult disease on the contralateral side in (a): level I and (b): level II for various clinical diagnoses (lymph involvement and T-category)

However, we have to consider the midline extension as an important risk factor. The predicted risk of occult disease in contralateral level I and II, additionally stratified for midline extension, is displayed in figure 4.9. The risks when no midline extension is diagnosed are very low and almost equal to the overall risks shown in 4.8 as only around 17% of all tumors extend over the midline. As soon as the clinical diagnose includes midline extension of the tumor, the risk of occult disease in the contralateral levels I and II increases drastically to around 4-5%. So neither the ipsilateral involvement nor the T-category is predicted to have a significant influence on the risk but the midline extension does. Summarizing, it can be said that a patient without midline extension and only clinical diagnosed ipsilateral involvement could be suitable for unilateral neck treatment. For patients with midline extension, caution is advised due to the significant increase in risk for contralateral microscopic metastases.

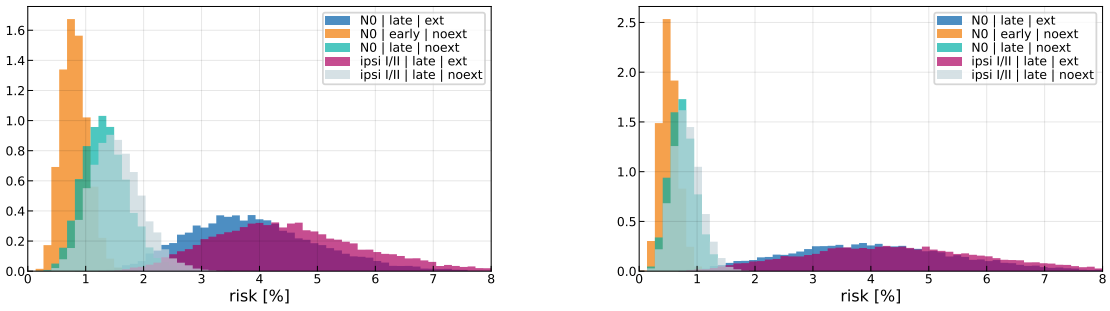

(a) (b)

Figure 4.9: Histogram showing the risk of occult disease in (a): level I and (b): level II on the contralateral side for various clinical diagnoses also including midline extension.

4.4 Model evaluation and comparison

The bilateral models, one incorporating simple marginalization over midline extension and the other accounting for the possible time evolution of the midline extension, showed negligible differences in the prevalence and risk predictions analyzed in the previous section 4.3. However, to compare the model approaches in a mathematical way, the model evidence provides the needed information. The higher the value of the model evidence the better a model describes the given data. This does not give us the possibility to independently rate a model but to compare it to other.

So mathematically speaking, we want to know which model $\mathcal{M}$ has the highest probability given the dataset $\boldsymbol{\mathcal{Z}}$. In Bayesian terms we can write this probability the following way:

$$P(\mathcal{M} \mid \boldsymbol{\mathcal{Z}}) = \frac{P(\boldsymbol{\mathcal{Z}} \mid \mathcal{M})P(\mathcal{M})}{P(\boldsymbol{\mathcal{Z}})} \tag{4.21}$$

Since we only have two models in the described case we can compute the Bayes factor to compare them if we assume a uniform prior $P(\mathcal{M})$. A uniform prior means that we a priori consider all models to have the same probability. The formula for the Bayes factor is:

$$K_{1\mathrm{v}2} = \frac{P\left(\mathcal{M}_1 \mid \boldsymbol{\mathcal{Z}}\right)}{P\left(\mathcal{M}_2 \mid \boldsymbol{\mathcal{Z}}\right)} = \frac{P\left(\boldsymbol{\mathcal{Z}} \mid \mathcal{M}_1\right) P\left(\mathcal{M}_1\right)}{P\left(\boldsymbol{\mathcal{Z}} \mid \mathcal{M}_2\right) P\left(\mathcal{M}_2\right)} = \frac{P\left(\boldsymbol{\mathcal{Z}} \mid \mathcal{M}_1\right)}{P\left(\boldsymbol{\mathcal{Z}} \mid \mathcal{M}_2\right)} \tag{4.22}$$

On the right hand side of the equation we now have the model evidences of the two models we want to compare. We can write them as their respective likelihoods, marginalized over all parameters:

$$P(\boldsymbol{\mathcal{Z}} \mid \mathcal{M}) = \int P(\boldsymbol{\mathcal{Z}} \mid \theta, \mathcal{M}) P(\theta \mid \mathcal{M}) d\theta \tag{4.23}$$

Normally, no analytical solution exists for this integral and due to the number of model parameters it is also almost impossible to brute force calculate the integral. So several approximation methods to calculate the model evidence have been developed. In this case we will use thermodynamic integration that is possible in the context of Markov-Chain Monte Carlo sampling used for the training process of our model. We will not introduce the mathematical background here but a short introduction of the concept can be found in [13] and for further background [44] is recommended.

In table 4.1 the log-evidence and its standard deviation can be found for the two models.

Model	log-evidence	standard deviation
Simple marginalization	-952.00	1.87
Time evolution	-936.93	1.98

Table 4.1: Log-evidence and the standard deviation for the two compared models that incorporate the marginalization over the midline extension and the time evolution of the midline extension.

Using eq. 4.22 we get a Bayes factor in the order of $\sim 10^6$. According to [45] a Bayes factor of larger than 10^2 is decisive. So in our case this means that the time evolution model is more strongly supported by the data under the consideration of the simple marginalization model with decisive strength. Therefore we can conclude that the advantage of the model including the time evolution of the midline extension can not visually be determined to be more strongly supported by the data but a statistical analysis shows the expected benefits of the more general and sophisticated approach to model and include the midline extension state.

However, this evaluation has to be regarded with suspicion as further analysis is needed on the exact comparability of the likelihood of the two models as the midline extension information is not handled in the same way.

Chapter 5

Discussion of model-based results

In the previous chapter 4 we have shown that the hidden Markov model proposed by Ludwig et al. [1] can be extended to also deal with missing midline extension information. Additionally, a general approach to model the midline extension evolution over time has been introduced and incorporated into the existing model. The bilateral model with the proposed extensions regarding the midline extension and also the existing unilateral model have been tested on the whole OCSCC dataset including pathological information of lymph node involvement for LNL I-V for 348 patients treated at the Centre Léon Bérard and the Inselspital Bern. All three tested models showed good capability to describe the lymphatic metastatic progresseion respectively the patient's evolution over time for the ipsilateral (unilateral and bilateral model) and contralateral (bilateral model) side of the neck. Therefore, we have the ability to reliably predict the prevalence for the involvement of individual LNLs or patterns of lymph node involvement that was also observed in the multicentric dataset. It is also possible to quantify the influence of the patient's T-category and midline extension state on the progression of the lymph node involvement, however, also because of the restricted flexibility of the model regarding the number of model parameters, some Limitations arise. These include over- or underestimation of the observed prevalence for early and late T-category patients. A combination of the T-category with clinically diagnosed involvement (N-category) could be a possible solution to this by reducing the sole dependence on the T-category. The influence of the midline extension on the contralateral spread seems to be slightly overestimated as well but because of the limited available data further testing with a larger dataset would be needed to further elaborate on this matter. Nonetheless, the T-category and midline extension are important risk factors regarding the lymph node involvement and therefore are also valuable for a subsequent risk prediction based on different clinical diagnoses.

The most important capability of the hidden Markov model is the possibility of risk predictions for occult disease in the individual LNLs given a specific clinical diagnosis.

This allows a highly diagnosis specific assessment of the CTV-N definiton that is not implemented in current guidelines that are mainly based on the TNM classification [40]. The performed risk predictions for the contralateral and ipsilateral neck indicate the possibility of a more elective CTV-N definition than recommended by current guidelines which at least support irradiation of level I, II and III on both sides of the neck [40]. Specifically, on the ipsilateral side treatment of level III could possibly be left untreated if a patient has no clincally diagnosed lymph metastases or even in the case of clinical involvement of level I (risk $< 3\%$). On the contralateral side an even larger deviation from the recommended irradiation of level I-III is supported by the model's risk predictions for occult disease. The predicted risks are below 2% given any clinical diagnosis on the ipsilateral side when the tumor is not extending over the mid-saggital plane. Therefore, a unilateral treatment for OCSCC patients without diagnosed midline extension of the primary tumor could be taken into account.

Training the model on a dataset that mainly includes pathological data increases the credibility of the model's training process and it's predictions. However, there are still some limitations and potential sources of bias regarding the data. At both institutions some patients received modified neck dissections which means that for example contralateral neck dissection was not performed in all patients. This could potentially lead to an underestimation of the prevalence of occult metastases in these contralateral levels. Additionally, it has to be mentioned that the dataset is based on information acquired during routine clinical treatment and could therefore be inherent across the institutions including uncertainty in the separation of individual LNLs. An evidence for this could be the difference in involvement of level III and V between the ISB and CLB dataset. Patients from the Inselspital Bern have lower involvement in level V than in the CLB dataset but higher involvement and more investigated lymph nodes in level III, indicating the mentioned inaccuracies. Finally, both datasets only contain patients who received neck dissection and patients treated with definitive radiotherapy are excluded. Since the primary treatment at both institutions included surgery, this should not lead to a strong patient selection bias.

The introduced time evolution of the midline extension provided a more general approach to model the patient's evolution and deal with missing midline extension information. In addition, an extension of the model to take the various subsites into account would be an interesting next step. This could improve the model by being able to account for the shown systematic differences in the lymphatic spread from the individual subsites. Finally, a redefinition of the T-category dependence by additionally including some lymph node involvement information into the time prior could adress the limitation of over- or underestimating the prevalence in certain scenarios stratified for T-category.

Chapter 6

Conclusion

This thesis presents an extensive analysis of the lymph node involvement patterns of OCSCC patients and e.g presented primary tumor location specific spread pattern characteristics or the dependence on various clinicopathological risk factors such as T-category, extracapsular extension or midline extension. The subsequent application of a hidden Markov model to model and describe the lymphatic metastatic progression including the developed model extensions could be analysed in detail on the basis of these descriptive statistics. However, it also includes a general overview that future studies could benefit from by giving additional information for example about the influence of ECE on the lymph involvement.

The application and testing of the hidden Markov model showed that it can also describe a OCSCC patient's evolution via lymphatic spread over time well. Based on the model's risk predictions for occult disease given a specific clinical diagnosis a more personal CTV-N definition can be made, potentially allowing volume de-escalation strategies by e.g sparing ipsilateral LNL III for a clinically classified N0 patient and contralateral LNLs in patients without a primary tumor extending over the mid-saggital plane.

Bibliography

[1] Roman Ludwig et al. "A hidden Markov model for lymphatic tumor progression in the head and neck". In: *Scientific Reports 2021 11:1* 11.1 (June 2021), pp. 1–17. ISSN: 2045-2322. DOI: 10.1038/s41598-021-91544-1. URL: https://www.nature.com/articles/s41598-021-91544-1.

[2] Barbora Peltanova, Martina Raudenska, and Michal Masarik. "Effect of tumor microenvironment on pathogenesis of the head and neck squamous cell carcinoma: A systematic review". In: *Molecular Cancer* 18.1 (2019), pp. 1–24. ISSN: 14764598. DOI: 10.1186/s12943-019-0983-5.

[3] Bernard W. Stewart and Christopher P. Wild. "World Cancer Report 2014". In: (2014).

[4] D. M. Parkin et al. "Global Cancer Statistics, 2002". In: *CA: A Cancer Journal for Clinicians* 55.2 (2005), pp. 74–108. ISSN: 0007-9235. DOI: 10.3322/canjclin.55.2.74.

[5] David G Pfister et al. "Head and Neck Cancers, Version 2.2014". In: *Journal of the National Comprehensive Cancer Network* 12.10 (Oct. 2014), pp. 1454–1487. ISSN: 1540-1405. DOI: 10.6004/jnccn.2014.0142. URL: www.smokefree.org.%20https://jnccn.org/doi/10.6004/jnccn.2014.0142.

[6] Shu Chun Chuang et al. "Risk of second primary cancer among patients with head and neck cancers: A pooled analysis of 13 cancer registries". In: *International Journal of Cancer* 123.10 (2008), pp. 2390–2396. ISSN: 00207136. DOI: 10.1002/ijc.23798.

[7] Rosemary Martino and Jolie Ringash. "Evaluation of Quality of Life and Organ Function in Head and Neck Squamous Cell Carcinoma". In: *Hematology/Oncology Clinics of North America* 22.6 (Dec. 2008), pp. 1239–1256. ISSN: 08898588. DOI: 10.1016/j.hoc.2008.08.011. URL: https://linkinghub.elsevier.com/retrieve/pii/S0889858808001238.

[8] J. A. Woolgar. "The topography of cervical lymph node metastases revisited: the histological findings in 526 sides of neck dissection from 439 previously untreated patients". In: *International Journal of Oral and Maxillofacial Surgery* 36.3 (Mar. 2007), pp. 219–225. ISSN: 09015027. DOI: 10.1016/j.ijom.2006.10.014. URL: http://www.ijoms.com/article/S0901502706004814/fulltext%20http://www.ijoms.com/article/S0901502706004814/abstract%20https://www.ijoms.com/article/S0901-5027(06)00481-4/abstract.

[9] K. S.Clifford Chao et al. "Determination and delineation of nodal target volumes for head-and-neck cancer based on patterns of failure in patients receiving definitive and postoperative IMRT". In: *International Journal of Radiation Oncology Biology Physics* 53.5 (2002), pp. 1174–1184. ISSN: 03603016. DOI: 10.1016/S0360-3016(02)02881-X.

[10] Jatin P. Shah, Frank C. Candela, and Anil K. Poddar. "The patterns of cervical lymph node metastases from squamous carcinoma of the oral cavity". In: *Cancer* 66.1 (July 1990), pp. 109–113. ISSN: 0008-543X. DOI: 10.1002/1097-0142(19900701)66:1<109::AID-CNCR2820660120>3.0.CO;2-A. arXiv: arXiv:1011.1669v3. URL: https://onlinelibrary.wiley.com/doi/10.1002/1097-0142(19900701)66:1%7B%5C%%7D3C109::AID-CNCR2820660120%7B%5C%%7D3E3.0.CO;2-A.

[11] Ali Razfar et al. "Incidence and patterns of regional metastasis in early oral squamous cell cancers: Feasibility of submandibular gland preservation". In: *Head & Neck* 31.12 (Dec. 2009), pp. 1619–1623. ISSN: 10433074. DOI: 10.1002/hed.21129. URL: https://onlinelibrary.wiley.com/doi/10.1002/hed.21129.

[12] Bertrand Pouymayou et al. "A Bayesian network model of lymphatic tumor progression for personalized elective CTV definition in head and neck cancers". In: *Physics in Medicine & Biology* 64.16 (Aug. 2019), p. 165003. ISSN: 0031-9155. DOI: 10.1088/1361-6560/AB2A18. URL: https://iopscience.iop.org/article/10.1088/1361-6560/ab2a18%20https://iopscience.iop.org/article/10.1088/1361-6560/ab2a18/meta.

[13] Roman Ludwig. "Modelling Lymphatic Metastatic Progression in Head and Neck Cancer". PhD thesis.

[14] Sukhjeet S. Batth, Jimmy J. Caudell, and Allen M. Chen. "Practical considerations in reducing swallowing dysfunction following concurrent chemoradiotherapy with intensity-modulated radiotherapy for head and neck cancer". In: *Head & Neck* 36.2 (Feb. 2014), pp. 291–298. ISSN: 10433074. DOI: 10.1002/hed.23246. URL: https://onlinelibrary.wiley.com/doi/10.1002/hed.23246.

[15] Roman Ludwig et al. "Detailed patient-individual reporting of lymph node involvement in oropharyngeal squamous cell carcinoma with an online interface". In: *Radiotherapy and Oncology* 169 (Apr. 2022), pp. 1–7. ISSN: 0167-8140. DOI: 10.1016/J.RADONC.2022.01.035.

[16] Elaine Nicpon Marieb. *Human Anatomy and Physiology*. 3rd ed. 2995. ISBN: 978-0-8053-4281-9.

[17] Senel Sevda. "An Overview of Physical, Microbiological and Immune Barriers of Oral Mucosa". In: *Int. J. Mol. Sci* 22 (2021), p. 7821. DOI: 10.3390/ijms22157821.

[18] Cynthia L. Willard-Mack. "Normal Structure, Function, and Histology of Lymph Nodes". In: *Toxicologic Pathology* 34.5 (Aug. 2006), pp. 409–424. ISSN: 0192-6233. DOI: 10.1080/01926230600867727. URL: http://journals.sagepub.com/doi/10.1080/01926230600867727.

[19] Christoph Wissmann and Michael Detmar. "Pathways Targeting Tumor Lymphangiogenesis". In: *Clinical Cancer Research* 12.23 (Dec. 2006), pp. 6865–6868. ISSN: 1078-0432. DOI: 10.1158/1078-0432.CCR-06-1800. URL: https://dx.doi.org/10.1158/1078-0432.CCR-06-1800.

[20] Guillermo Oliver and Michael Detmar. "The rediscovery of the lymphatic system: old and new insights into the development and biological function of the lymphatic vasculature". In: *Genes & Development* 16.7 (Apr. 2002), pp. 773–783. ISSN: 0890-9369. DOI: 10.1101/GAD.975002. URL: http://genesdev.cshlp.org/content/16/7/773.full%20http://genesdev.cshlp.org/content/16/7/773.

[21] Osamu Ohtani and Yuko Ohtani. "Structure and function of rat lymph nodes". In: *Archives of Histology and Cytology* 71.2 (2008), pp. 69–76. ISSN: 0914-9465. DOI: 10.1679/aohc.71.69. URL: http://www.jstage.jst.go.jp/article/aohc/71/2/71%7B%5C_%7D2%7B%5C_%7D69/%7B%5C_%7Darticle.

[22] Vishram Singh. *Textbook of Anatomy Head, Neck, and Brain*. Volume III. 2017, pp. 247–249. ISBN: 9788131237274.

[23] K. T. Robbins et al. "Standardizing Neck Dissection Terminology: Official Report of the Academy's Committee for Head and Neck Surgery and Oncology". In: *Archives of Otolaryngology - Head and Neck Surgery* 117.6 (June 1991), pp. 601–605. ISSN: 0886-4470. DOI: 10.1001/archotol.1991.01870180037007. URL: http://archotol.jamanetwork.com/article.aspx?articleid=619715.

[24] Vincent Grégoire et al. "CT-based delineation of lymph node levels and related CTVs in the node-negative neck: DAHANCA, EORTC, GORTEC, NCIC, RTOG consensus guidelines". In: *Radiotherapy and Oncology* 69.3 (2003), pp. 227–236. ISSN: 01678140. DOI: 10.1016/j.radonc.2003.09.011.

[25] Barbora Peltanova, Martina Raudenska, and Michal Masarik. "Effect of tumor microenvironment on pathogenesis of the head and neck squamous cell carcinoma: a systematic review". In: *Molecular Cancer* 18.1 (Dec. 2019), p. 63. ISSN: 1476-4598. DOI: 10.1186/s12943-019-0983-5. URL: https://molecular-cancer.biomedcentral.com/articles/10.1186/s12943-019-0983-5.

[26] A. S. JONES et al. "THE LEVEL OF CERVICAL LYMPH NODE METASTASES: THEIR PROGNOSTIC RELEVANCE AND RELATIONSHIP WITH HEAD AND NECK SQUAMOUS CARCINOMA PRIMARY SITES". In: *Clinical Otolaryngology* 19.1 (Feb. 1994), pp. 63–69. ISSN: 1749-4478. DOI: 10.1111/j.1365-2273.1994.tb01150.x. URL: https://onlinelibrary.wiley.com/doi/10.1111/j.1365-2273.1994.tb01150.x.

[27] Young Chang Lim et al. "Distributions of Cervical Lymph Node Metastases in Oropharyngeal Carcinoma: Therapeutic Implications for the N0 Neck". In: *The Laryngoscope* 116.7 (July 2006), pp. 1148–1152. ISSN: 0023-852X. DOI: 10.1097/01.mlg.0000217543.40027.1d. URL: https://onlinelibrary.wiley.com/doi/10.1097/01.mlg.0000217543.40027.1d.

[28] Robert P Takes. "Staging of the neck in patients with head and neck squamous cell cancer: Imaging techniques and biomarkers". In: *Oral Oncology* 40.7 (Aug. 2004), pp. 656–667. ISSN: 13688375. DOI: 10.1016/j.oraloncology.2003.11.001. URL: https://linkinghub.elsevier.com/retrieve/pii/S1368837503002367.

[29] Roman Ludwig. *LyProX*. 2023. URL: https://lyprox.org.

[30] World Health Organization. *International classification of diseases for oncology (ICD-O)*. 3rd ed., 1. World Health Organization, 2013, viii, 242 p.

[31] Francis Deng, Andrew Murphy, and Daniel J. Bell. *Extranodal extension*. 2019. DOI: https://doi.org/10.53347/rID-66438. URL: https://radiopaedia.org/articles/66438.

[32] Julian Biau et al. "Selection of lymph node target volumes for definitive head and neck radiation therapy: a 2019 Update". In: *Radiotherapy and Oncology* 134 (May 2019), pp. 1–9. ISSN: 0167-8140. DOI: 10.1016/J.RADONC.2019.01.018. URL: http://www.thegreenjournal.com/article/S0167814019300234/fulltext%20http://www.thegreenjournal.com/article/S0167814019300234/abstract%20https://www.thegreenjournal.com/article/S0167-8140(19)30023-4/abstract.

[33] Christopher M. Bishop. *Pattern Recognition and Machine Learning*. New York: Springer, 738 pp. ISBN: 978-0-387-31073-2.

[34] David J C MacKay. *Information Theory, Inference, and Learning Algorithms*, 640 p.

[35] Andrew Gelman et al. *Bayesian Data Analysis*. Chapman and Hall/CRC, Nov. 2013, 675 pp. ISBN: 9780429113079. DOI: 10.1201/b16018. URL: https://www.taylorfrancis.com/books/9781439898208.

[36] Daniel Foreman-Mackey et al. "emcee : The MCMC Hammer ". In: *Publications of the Astronomical Society of the Pacific* 125.925 (2013), pp. 306–312. ISSN: 00046280. DOI: 10.1086/670067. arXiv: 1202.3665.

[37] Cajo J. F. ter Braak and Jasper A. Vrugt. "Differential Evolution Markov Chain with snooker updater and fewer chains". In: *Statistics and Computing* 18.4 (Dec. 2008), pp. 435–446. ISSN: 0960-3174. DOI: 10.1007/s11222-008-9104-9. URL: http://link.springer.com/10.1007/s11222-008-9104-9.

[38] Benjamin E Nelson, Eric B Ford, and Matthew J Payne. *RUN DMC: AN EFFICIENT, PARALLEL CODE FOR ANALYZING RADIAL VELOCITY OBSERVATIONS USING N-BODY INTEGRATIONS AND DIFFERENTIAL EVOLUTION MARKOV CHAIN MONTE CARLO*. Tech. rep. 2013. arXiv: 1311.5229v1.

[39] A. Al-Mamgani, M. Verheij, and M.W.M. van den Brekel. "Elective unilateral nodal irradiation in head and neck squamous cell carcinoma: A paradigm shift". In: *European Journal of Cancer* 82 (Sept. 2017), pp. 1–5. ISSN: 09598049. DOI: 10.1016/j.ejca.2017.05.035. URL: https://linkinghub.elsevier.com/retrieve/pii/S0959804917309991.

[40] Vincent Grégoire et al. "Target volume selection and delineation (T and N) for primary radiation treatment of oral cavity, oropharyngeal, hypopharyngeal and laryngeal squamous cell carcinoma". In: *Oral Oncology* 87.November (2018), pp. 131–137. ISSN: 18790593. DOI: 10.1016/j.oraloncology.2018.10.034. URL: https://doi.org/10.1016/j.oraloncology.2018.10.034.

[41] Julian Biau et al. "Selection of lymph node target volumes for definitive head and neck radiation therapy: a 2019 Update". In: *Radiotherapy and Oncology* 134 (May 2019), pp. 1–9. ISSN: 01678140. DOI: 10.1016/j.radonc.2019.01.018. URL: https://linkinghub.elsevier.com/retrieve/pii/S0167814019300234.

[42] Pieter D. de Veij Mestdagh et al. "SPECT/CT-guided elective nodal irradiation for head and neck cancer is oncologically safe and less toxic: A potentially practice-changing approach". In: *Radiotherapy and Oncology* 147 (June 2020), pp. 56–63. ISSN: 01678140. DOI: 10.1016/j.radonc.2020.03.012. URL: https://linkinghub.elsevier.com/retrieve/pii/S0167814020301213.

[43] Pieter D. de Veij Mestdagh et al. "Incidence of contralateral regional failure in the electively irradiated contralateral neck of patients with head and neck squamous cell carcinoma". In: *Clinical and Translational Radiation Oncology* 17 (2019), pp. 7–13. ISSN: 24056308. DOI: 10.1016/j.ctro.2019.04.015. URL: https://doi.org/10.1016/j.ctro.2019.04.015.

[44] Eduardo A. Aponte et al. "An introduction to thermodynamic integration and application to dynamic causal models". In: *Cognitive Neurodynamics* 16.1 (Feb. 2022), pp. 1–15. ISSN: 1871-4080. DOI: 10.1007/s11571-021-09696-9. URL: https://link.springer.com/10.1007/s11571-021-09696-9.

[45] Harold Jeffreys. *The Theory of Probability*. 3rd ed. Oxford, 1998, p. 432. ISBN: 9780191589676.

Acknowledgements

I would like to thank Professor Jan Unkelbach without whom this project would not have been possible and always gave valuable inputs regarding and feedback. Special thanks go to Dr. Roman Ludwig who helped me a lot with the mathematical background, the computational implementations and made sure that the code, plots and Github repositories ended up looking way cleaner than the would have without his inverventions and tips and tricks.

Additionally, I want to thank Janic, Florian, Julian, Yoel, Esmée and Alice for their support on the project and motivating me a lot along the way.

Declaration

I hereby declare that this thesis is my original work and it has been written by me in its entirety. I have acknowledged all the sources of information which have been used in this thesis.

University of Zurich, September 2023

Lars Widmer